

CHAPTER IV

RESULTS AND DISCUSSION

4.1 Surface Characterization

The surface characterizations were conducted on steels with different Cr contents, i.e., A106B carbon steel (0.03%Cr), Qinshan steel (0.33%Cr) and 2.5%Cr / 1.0%Mo steel and 304 stainless steel (19.1%Cr). All the steels were pre-filmed in the simulated primary coolant system of CANDU reactor.

4.1.1 SEM/EDX Analysis

The surface morphology of the oxide film and the oxide particle size were analyzed by SEM micrograph. Figure 4.1 shows SEM micrographs in an overview of the surfaces of all oxide film forms on materials at 100X magnifications. It is seen that the oxide film on A106B steel, which contained the lowest Cr content, had a roughest surface compare with these on Qinshan steel, 2.5%Cr / 1.0%Mo Steel and 304SS. With increasing Cr content, the surface of oxide films became smoother. It can be assumed that a higher dissolution rate occurred in the steel specimens containing lower Cr, resulting in the rougher oxide surface.

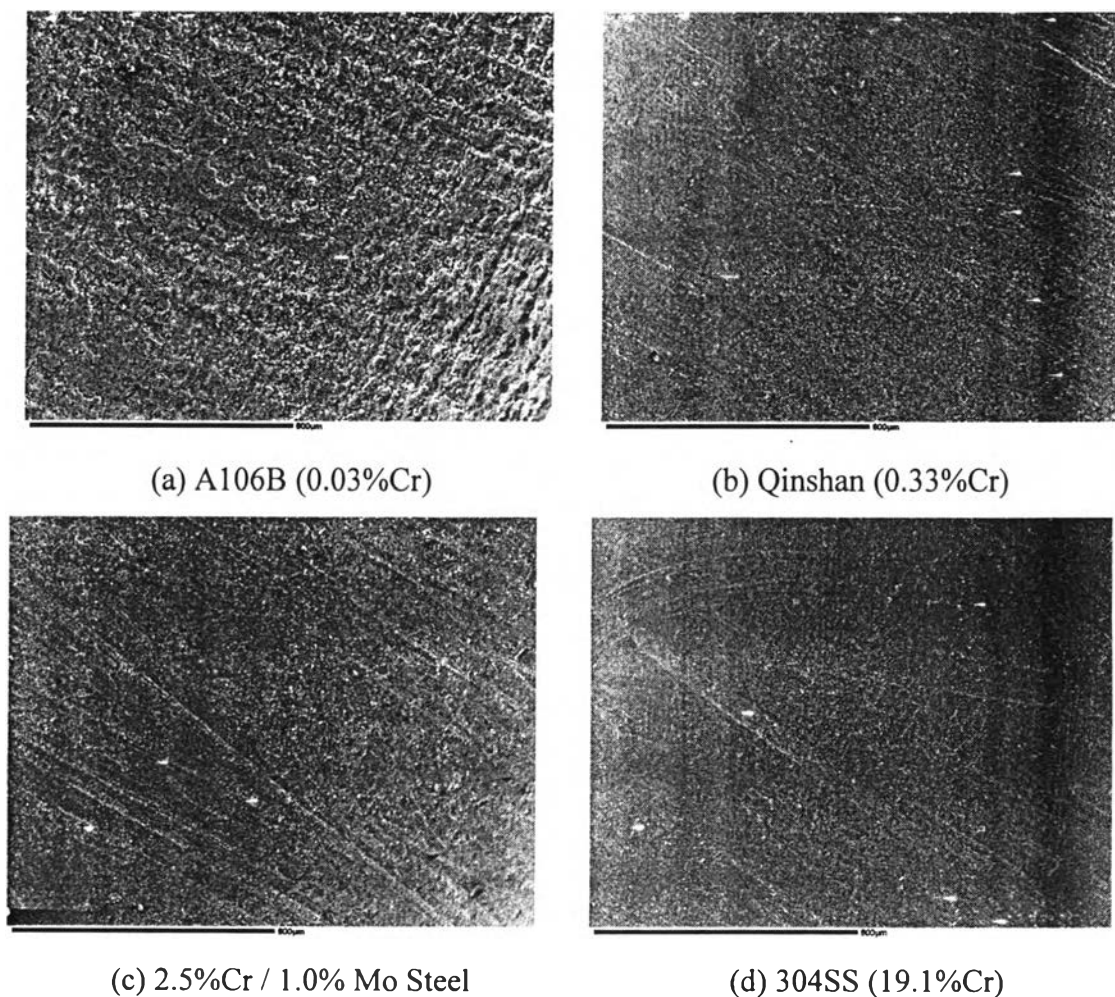


Figure 4.1 SEM micrograph of the oxide surface formed on different steel at 100X magnification.

The surface morphology of oxide films at higher resolution 10,000X at magnifications are shown in Figure 4.2. It is seen that all oxide film consisted of two with discrete size ranges of oxide particles. The large oxide particles overlay a layer of small particles. There are significant differences of the size and packing density of the oxide particle on different steels. The particle size distribution of the large and small oxide particles are summarized in Table 4.1.

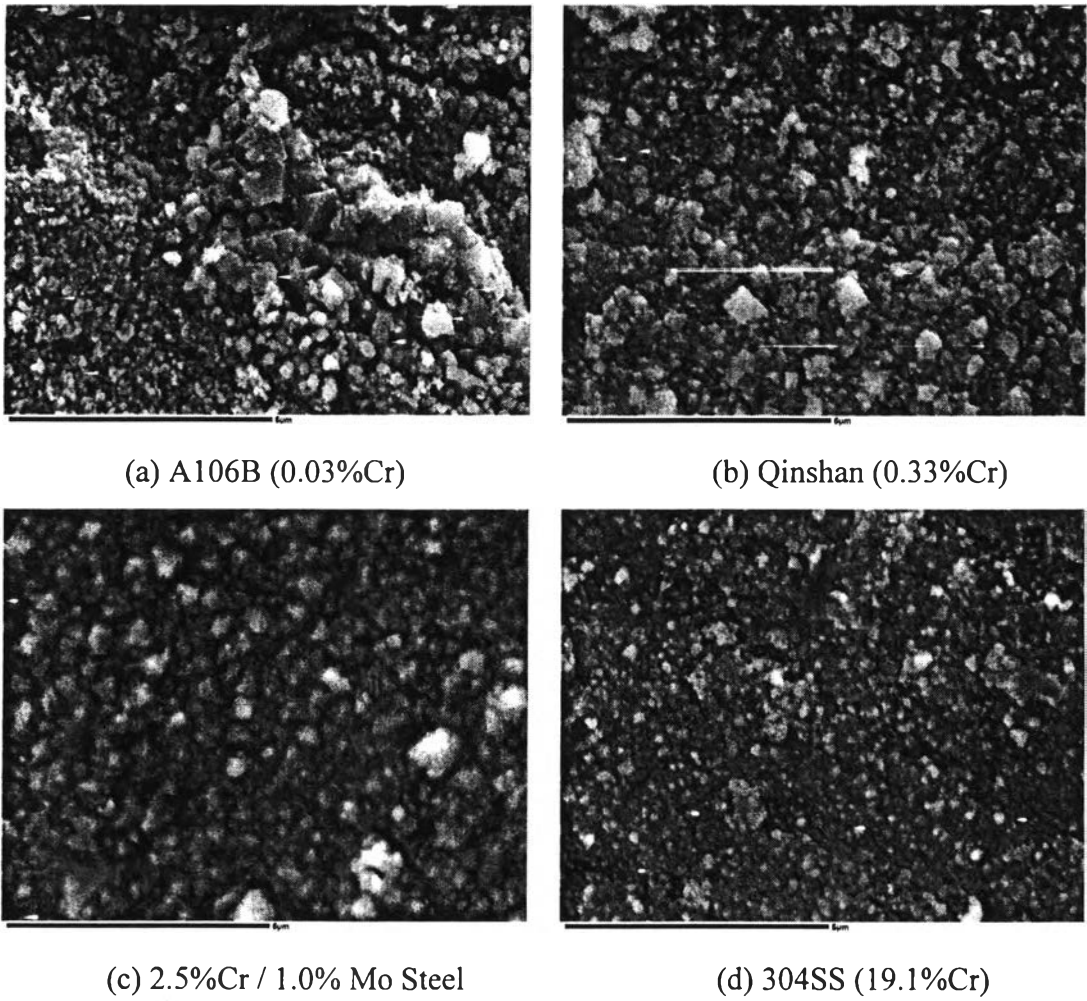


Figure 4.2 SEM micrographs of the oxide surface formed on different steel at 10,000X magnification.

Table 4.1 Size distribution of oxide particles on different steels

Type	Particle size (μm)	
	Large oxide particle	Small oxide particle (Fine grain layer)
A106B	0.9-1.0	0.18-0.21
Qinshan	0.7-0.93	0.07-0.09
2.5%Cr / 1.0%Mo Steel	0.55-0.78	0.06-0.11
304 SS	0.32-0.48	N/A

Table 4.1 shows that the specimens with a higher Cr content had a relatively smaller size for both particles, resulting in a higher packing density or a more compact layer. While, the oxide particles on A106B were the largest, those on 304SS were the smallest in terms of dimensional size.

Apparently, the morphology of the oxide films is changed with the Cr content of steels. A higher Cr content enhanced the packing density of the oxide film.

It is observed that the oxide film consisted of two kinds of particles with different size ranges. EDX analysis was performed on both particles and the results are shown in Table4.2

Table 4.2 EDX analysis of large particle and small particles on different Steels

Atomic%	A106B		Qinshan Steel		2.5%Cr / 1.0%Mo Steel		304SS	
	Small particle	Large particle	Small particle	Large particle	Small particle	Large particle	Small particle	Large particle
Si	0.43	0.29	0.64	0.52	0.28	0.20	0.66	0.51
Mo	-	-	-	-	0.12	0.04	-	-
Ti	0.16	0.36	0.25	0.40	0.19	0.48	0.17	0.22
Cr	0.17	0.09	0.67	0.47	1.27	0.93	15.26	14.05
Mn	0.12	0.07	0.29	0.20	0.11	0.03	0.56	0.35
Fe	40.58	37.02	39.26	35.04	39.59	33.84	21.77	20.66
Ni	2.24	5.03	3.41	5.55	3.09	6.83	7.35	6.64
O	56.31	57.14	55.48	57.83	55.35	57.65	54.23	57.58

It is seen that Ti and Ni present in both layers, although Fe-Cr alloy matrixes did not originally contain nickel (Ni) and titanium (Ti) as the main composition. The Ni and Ti contamination may be from the loop components such as Hastelloy autoclave (56% Ni).

For all oxide films on A106B carbon steel and Fe-Cr alloys, a higher Cr was detected on the small particles rather than on the large particles. In other words, the inner layers contained more Cr than the outer layer. The high oxygen concentration of the small particles indicated the EDX did not pick up the interference signal from the underlying steel matrix. Trace amounts of Si and Mn were also detected in the oxide film. The oxide particles on 2.5%Cr / 1.0%Mo steel also detected Mo, which could be from the steel matrix.

When normalizing the concentrations of main elements (Fe, Cr and Ni) relative to oxygen, the crystal structure of the oxide film could be roughly determined. Table 4.3 shows the ratio of Fe, Cr and Ni to O concentration. It is seen that the ratios Fe, Cr and Ni to O content of both particles sizes were close to 3, which indicates a spinel structure (AB_2O_4).

Table 4.3 Normalized concentration of Fe, Cr and Ni to O ratio

	A106B		Qinshan Steel		2.5%Cr / 1.0%Mo Steel		304SS	
	Small particle	Large particle	Small particle	Large particle	Small particle	Large particle	Small particle	Large particle
Fe	2.88	2.59	2.83	2.42	2.86	2.35	1.61	1.44
Cr	0.01	0.01	0.05	0.03	0.09	0.06	1.13	0.98
Ni	0.16	0.35	0.25	0.38	0.22	0.47	0.54	0.46
Total	3.05	2.95	3.12	2.84	3.18	2.89	3.27	2.87

4.1.2 TEM Analysis

All samples for TEM analysis were prepared by “Lift Out” technique, which is the technique that applies to the ion beam of gallium (Ga^+) to polish the working area (See Appendix C). The sample must be thinned until achieves electron transparent. The normal working thickness is between 120 to 500 nm.

4.1.2.1 A106B Carbon Steel

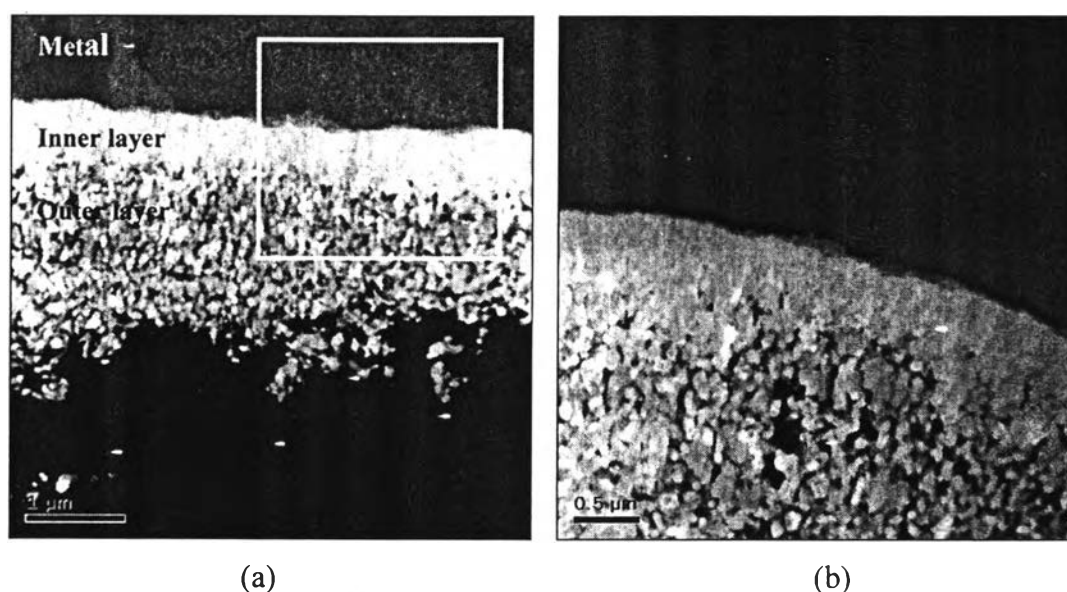
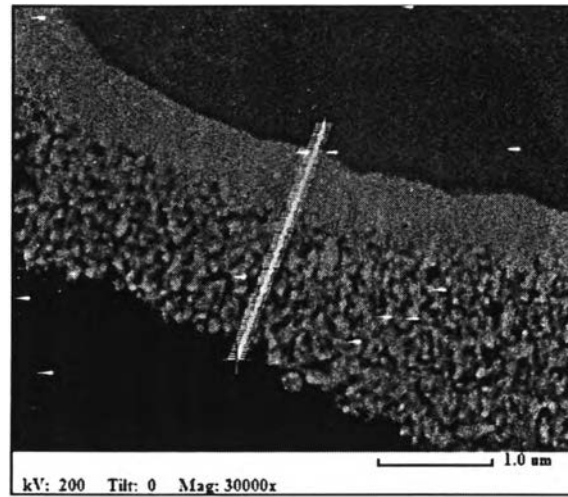
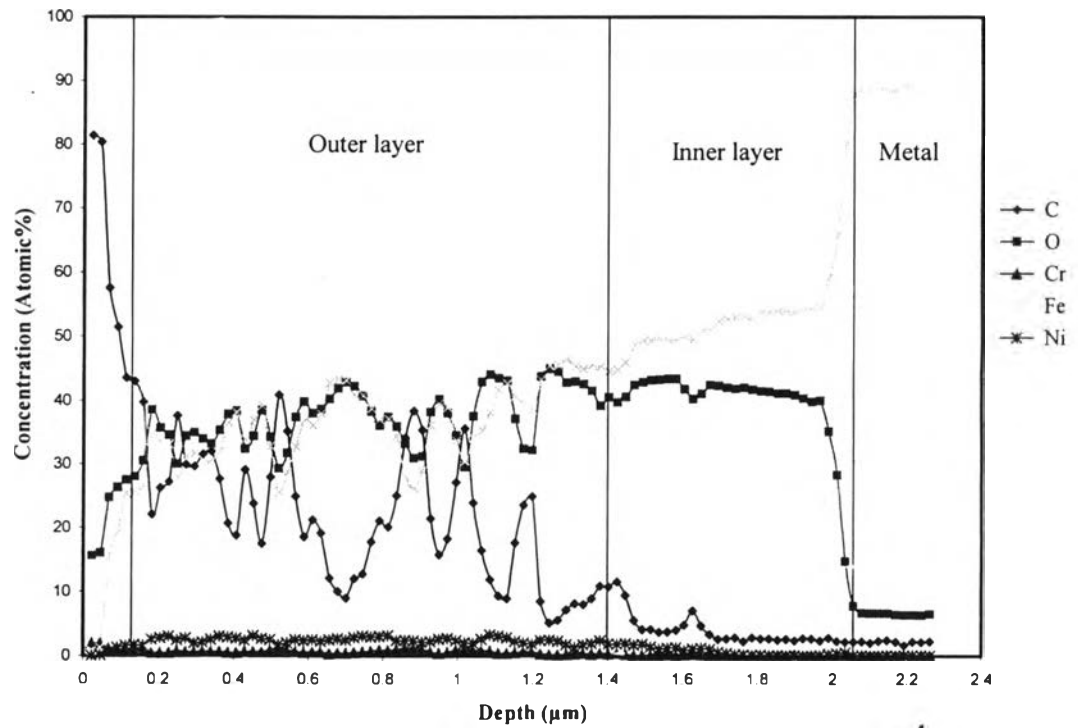


Figure 4.3 TEM micrographs showing the oxide film on A106B Carbon Steel.
(a) TEM micrograph in overview (b) TEM of square area shown in (a)

Figure 4.3a shows the micrograph of A106B specimen in overview. It clearly shows that the oxide film consisted of two different layers with different packing density. From Figure 4.3b, an outer oxide layer with relatively larger particles and an inner layer with finer particles are observed. Apparently, the packing density of the inner layer is greater than that of the outer layer.



(a)



(b)

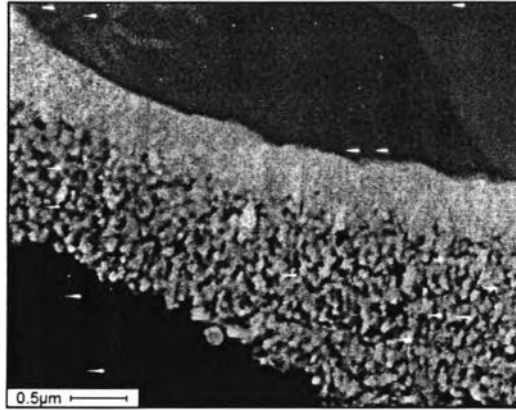
Figure 4.4 Line scanning result of A106B Carbon Steel.

(a) TEM micrograph with annotated line. (b) Depth profile of metal through the oxide layer.

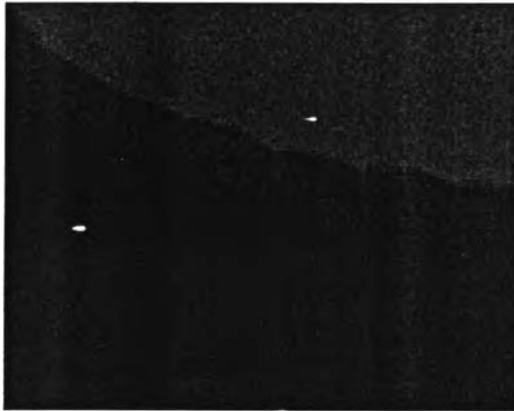
Figure 4.4b shows the concentration depth profile scanned from metal through the oxide layer with the scanning path shown in Figure 4.4a. The metal/oxide interface could clearly be indicated by a suddenly increase of oxygen and also drop of Fe content. The fluctuation of carbon concentration in the outer oxide was attributed to the loose structure. Carbon is one of the main compositions in epoxy, which was used to adhere the oxide during ion thinning. In addition the elements showed in Figure 4.4b, P, S, Si, Ti and Mn were also found in the oxide film. However, their concentrations were so low ($< 1\%$) that they are negligible.

The concentration depth profile can also be presented by EDX mapping. The darker colour level indicates the greater specie concentration. The comparison of colour level can be applied only for the same element.

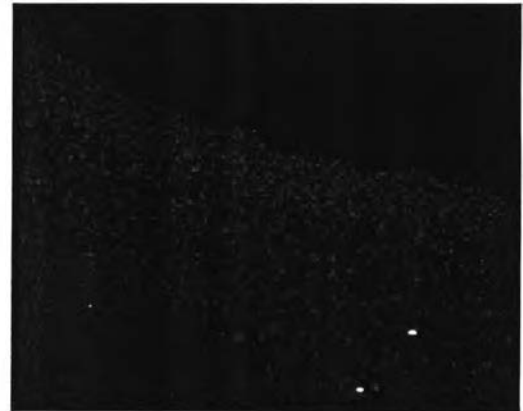
The Fe map in Figure 4.5 shows a sharp metal/oxide interface, while the O map confirmed that the identified inner and outer oxide, are indeed oxide. The Cr map indicated approximately equal concentration of chromium in inner and outer oxide layer. The Ni map shows the enrichment of nickel in the outer oxide layer.



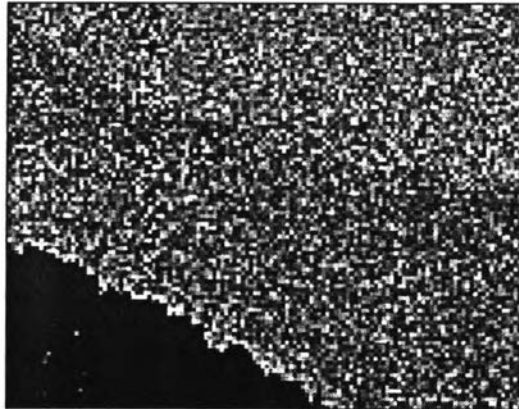
(a) Image



(b) Iron



(c) Oxygen



(d) Chromium



(e) Nickel

Figure 4.5 EDX mapping of A106B Carbon Steel.

a) Inner Layer

The concentration profile in Figure 4.4b and the EDX map in Figure 4.5b revealed an iron-rich oxide in this layer. The inner oxide was about $0.56\ \mu\text{m}$ thick. The maximum of iron concentration was about 55 percent at the metal/oxide interface and then depleted toward the outside surface. The oxygen concentration was quite constant at about 42 percent, nevertheless the oxygen concentration was not reliable. The TEM sample holder is made of copper. The Cu peak can overlap with the oxygen peak in the EDX spectrum, resulting in an error for calculating the oxygen concentration.

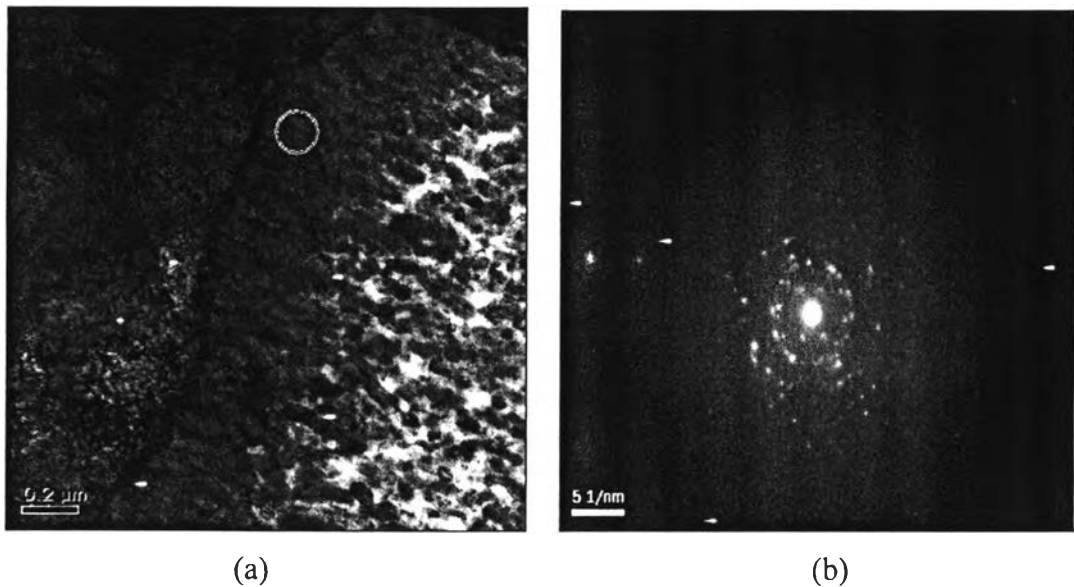


Figure 4.6 TEM micrograph of inner oxide layer with electron diffraction pattern of oxide layers developed on A106B_IN_2.

(a) TEM micrograph

(b) Diffraction pattern of circle area

Figure 4.6 shows the electron diffraction pattern of one of the selected points in the inner oxide layer. The electron diffractions of the fine grain, continuous layer as marked in the circle area were measured. The d-spacing of the spotty ring pattern was used to identify the crystal structure. All d-spacing values of diffraction point at the selected points are summarized in Table 4.4.

Table 4.4 The d-spacing values of the inner layer on A106B carbon steel

Specimen No.	d-Spacing Value (nm)						
A106B_IN_1	-	0.2970	0.2540	-	-	0.1625	0.1498
A106B_IN_2	0.4934	0.3038	0.2569	0.2153	-	0.1658	0.1526
A106B_IN_3	0.4953	0.3016	0.2592	0.2176	0.1749	0.1654	0.1509
Average	0.4943	0.3008	0.2567	0.2164	0.1749	0.1645	0.1511

In comparison with the measured d-spacing values in Table 4.4 and the typical values corresponding to the spinel structure of Fe_3O_4 in Table 4.5, it is seen that the inner oxide layer on A106B carbon steel was the Fe_3O_4 .

Table 4.5 The d-spacing values and reflection plane indices (h, k, l) of Fe_3O_4 structure

(h, k, l)	1 1 0	2 2 0	3 1 1	2 2 2	4 0 0	4 2 2	5 1 1	4 4 0
d-Spacing Value (nm)	0.4850	0.2966	0.2530	0.2419	0.2096	0.1712	0.1614	0.1483

EDX results also indicate the presence of Cr and Ni in the inner layer. However, the average concentrations of Ni and Cr compared with Fe content were so low that they were negligible ($\text{Ni/Fe} = 0.014$, $\text{Cr/Fe} = 0.003$).

b) Outer Layer

Relatively single octahedral particles were found in the outer oxide layer. The film thickness of outer layer was about 1.25 μm .

Figure 4.7 shows the electron diffraction pattern of the outer oxide layer. The electron diffraction pattern of the polycrystalline group in Figure 4.7b was a good fit to the Fe_3O_4 type. The d-spacing of A106B_OUT_1 and another is summarized in Table 4.6.

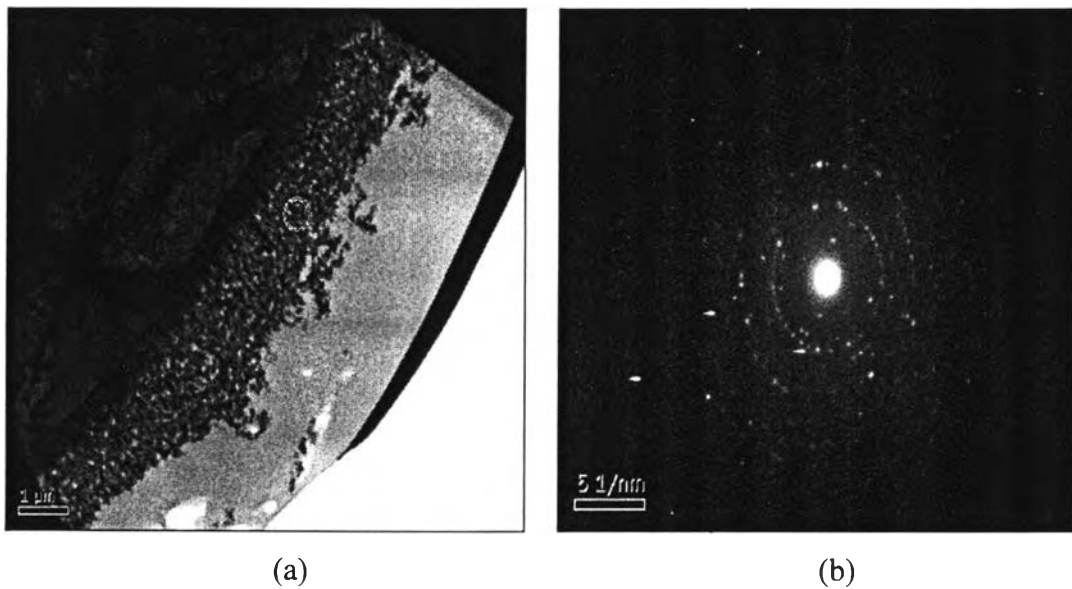


Figure 4.7 TEM micrograph of outer oxide layer with electron diffraction pattern of oxide layer developed on A106B_OUT_1.

(a) TEM micrograph (b) Diffraction pattern of a circle area shown in (a)

Table 4.6 The d-spacing values of the outer layer on A106B Carbon Steel

Specimen No.	d-Spacing Value (nm)						
A106B_OUT_1	0.4886	0.2965	0.2535	-	0.2100	0.1722	0.1618
A106B_OUT_2	0.4859	0.2942	0.2537	0.2492	0.2101	-	0.1624
Average	0.4872	0.2953	0.2536	0.2492	0.2100	0.1722	0.1621

The TEM cross sectional investigations in Figure 4.7 revealed the largest grain size of the outer oxide layer is generally about 0.16 μm . The large particle size (0.9-1.0 μm) from SEM observations probably detached from the surface during the oxide film-thinning step.

The EDX map in Figure 4.5e and the concentration depth profile in Figure 4.4b also showed the presence of higher Ni content in the oxide film. Ni is not an original composition of A106B. The source of nickel was probably from the loop components.

In summary, the crystal structure of oxide film formed on A106B carbon steel is mainly the Fe_3O_4 . Both the inner and outer oxide layers on A106B steel, regardless of particle size, are Fe_3O_4 .

The average ratios of Ni to Fe and Cr to Fe were 0.067 and 0.018, respectively. These values are quite low. Therefore, the crystal structure of oxide was mainly Fe_3O_4 . Therefore, it appears that both oxide layers of A106B, regardless of size, had the structure of Fe_3O_4 .

4.1.2.2 Qinshan Steel (0.33% Cr)

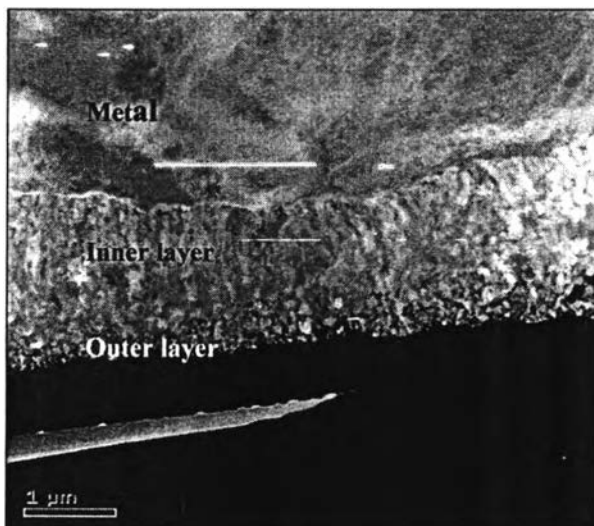
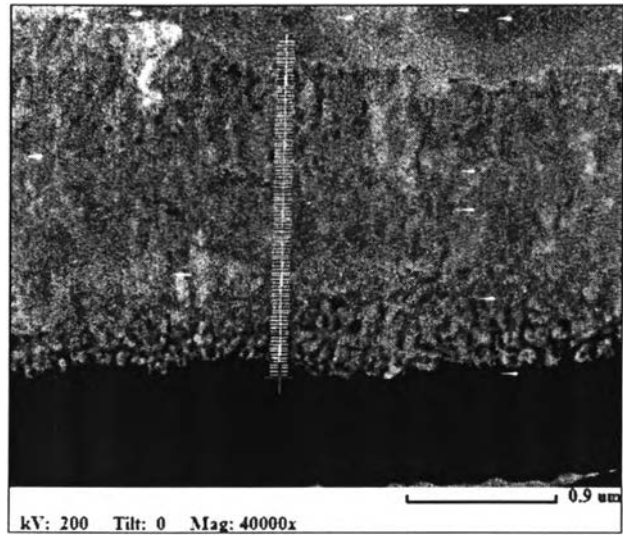


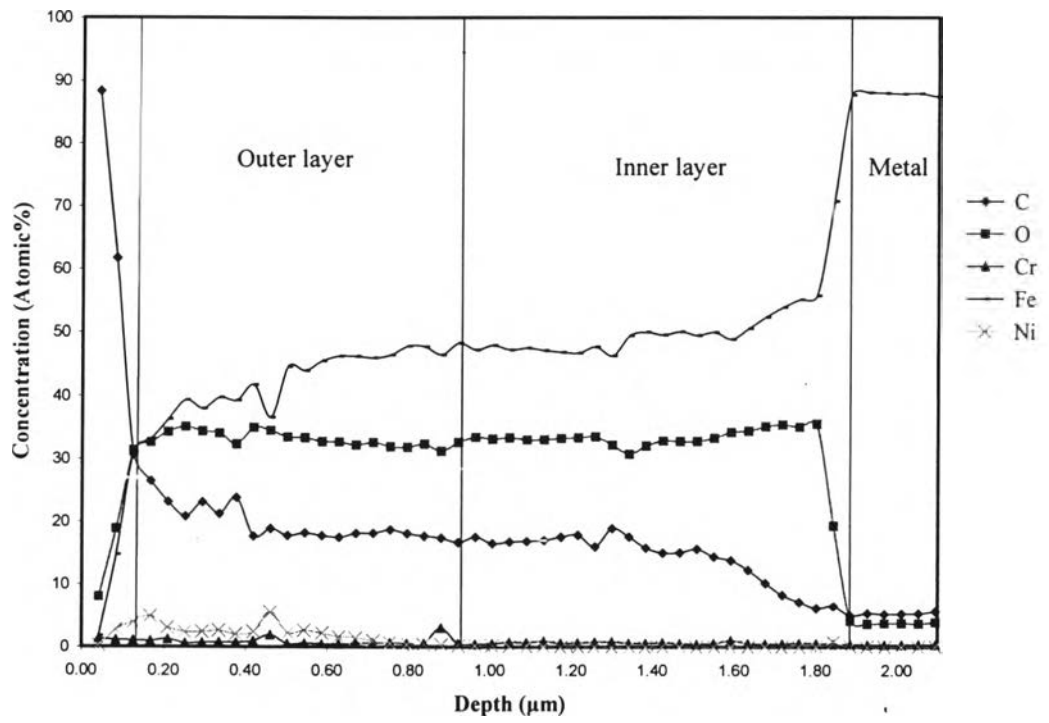
Figure 4.8 TEM micrograph showing the oxide film formed on Qinshan Steel.

Figure 4.8 shows the TEM micrograph of oxide film on Qinshan. The film included two different layers. The inner layer with fine grains and large particles of outer layer can be observed.

Figure 4.9 shows the concentration depth profile of the oxide film on Qinshan steel. The Fe concentration decreased continuously from inner to the outer oxide layer. The Cr concentration was very low and almost constant at 0.7 % for the inner layer and 0.8% for the outer layer. The contamination of Ni was observed at the outer layer (See Figure 4.10e). The relative concentration of each element can be visualized by the EDX map in Figure 4.10.



(a)

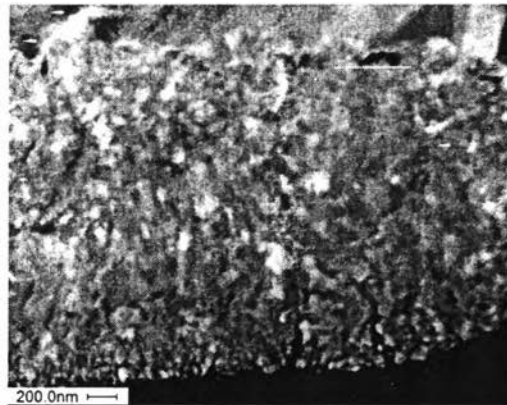


(b)

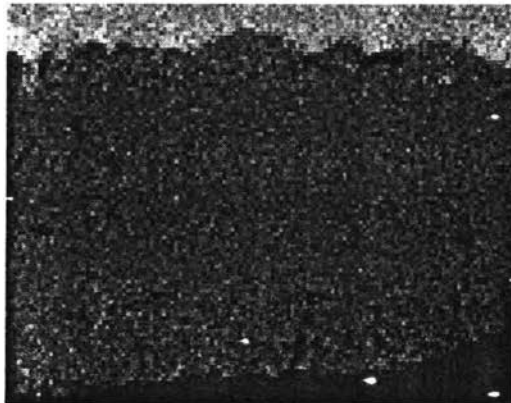
Figure 4.9 Line scanning result of Qinshan Steel.

(a) TEM micrograph with annotated line. (b) Depth profile from metal through the oxide layer

In the Figure 4.10, the Fe map shows a transition between the metal and oxide layer. The O map confirms that the identified inner and outer layers are indeed oxides. The Cr map indicates approximately equal concentration of chromium in the inner and outer oxide layer. The Ni map shows the enrichment of nickel contamination in the outer layer.



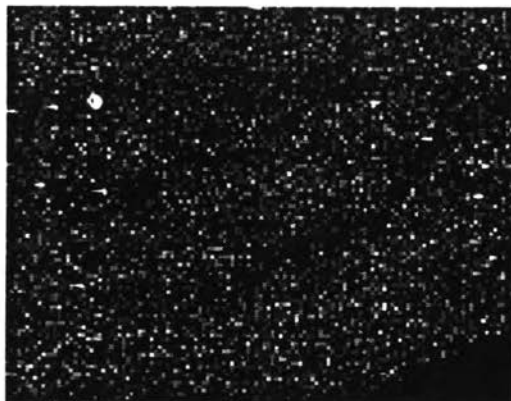
(a) Image



(b) Iron



(c) Oxygen



(d) Chromium



(e) Nickel

Figure 4.10 EDX mapping of Qinshan Steel.

a) Inner Layer

Based on the concentration depth profile in Figure 4.9b, the iron rich oxide can be observed. The ratio of the average concentrations of Cr to Fe was 0.013. The inner layer thickness was about 1.04 μm . The crystal structure of this fine grain layer can be identified from the diffraction pattern in Figure 4.11.

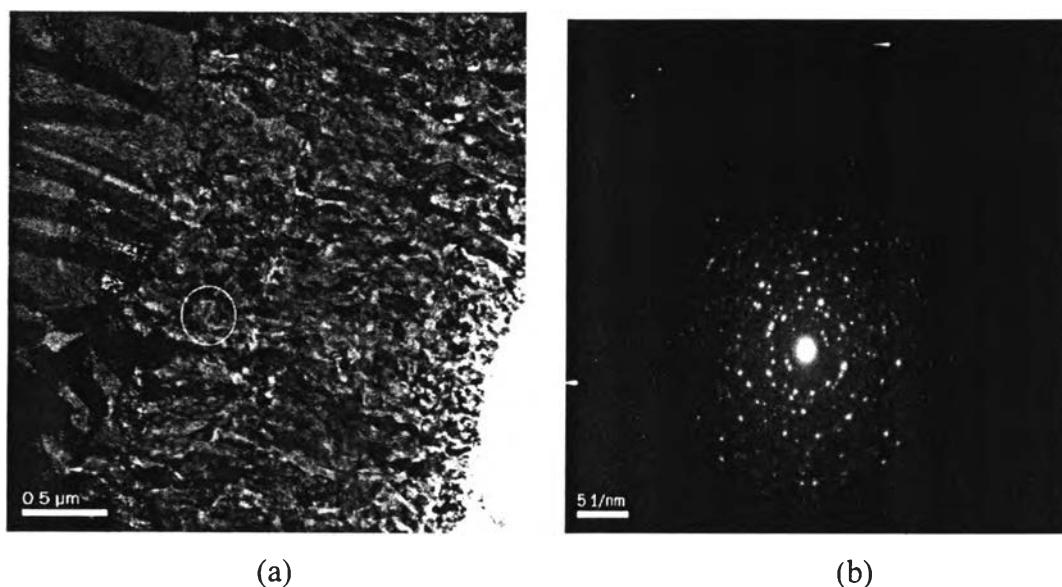


Figure 4.11 TEM micrograph of inner oxide layer with electron diffraction pattern of oxide layers developed on Qinshan_IN_3.

(a) TEM micrograph (b) Diffraction pattern of circle area

Figure 4.11 shows the diffraction patterns of the inner layer. The d-spacing values for various samples, which were utilized for identification of structure, are summarized in Table 4.7.

Table 4.7 The d-spacing values of the inner layer on Qinshan Steel

Specimen No.	d-Spacing Value (nm)						
Qinshan_IN_1	0.4869	0.2955	0.2548	0.2140	0.1726	0.1617	0.1491
Qinshan_IN_2	0.4837	0.2986	0.2544	0.2110	0.1714	0.1613	0.1485
Qinshan_IN_3	0.4856	0.2986	0.2537	0.2105	0.1736	0.1616	0.1506
Average	0.4854	0.2976	0.2543	0.2118	0.1725	0.1615	0.1494

The d-spacing values in Table 4.7 correspond to those of inverse spinel of Fe_3O_4 as shown Table 4.5. However, the depth profile in Figure 4.7, shows the presence of chromium ($\text{Cr}/\text{Fe} = 0.013$) which could substitute some of Fe^{3+} in the spinel structure.

b) Outer Layer

Similar to the previous specimen, the greater contamination of nickel can be observed on this layer. The ratio of Ni to Fe was of 0.052 on average.

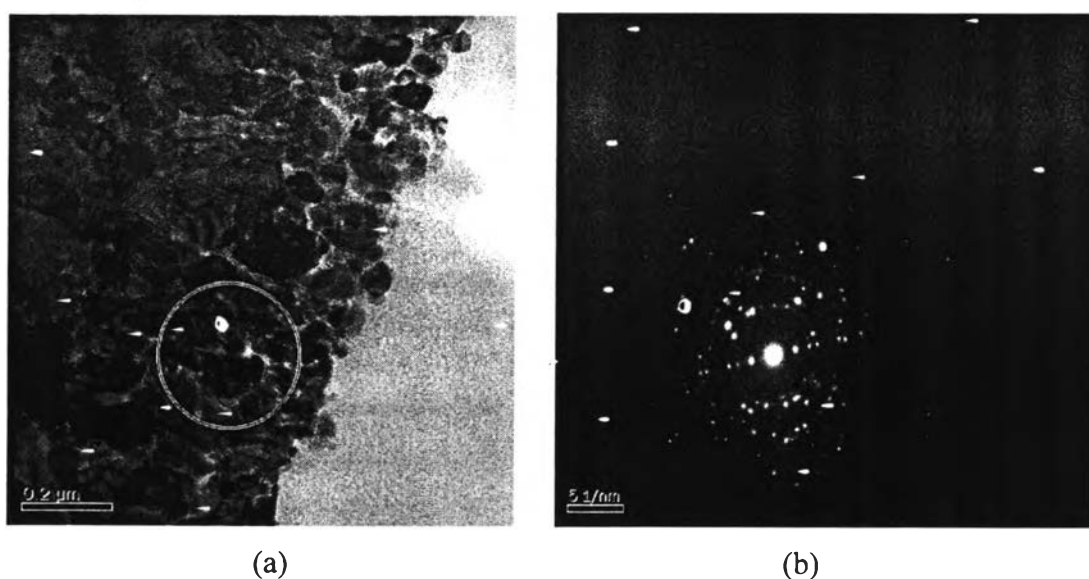


Figure 4.12 TEM micrograph of outer oxide layer with electron diffraction pattern of oxide layers developed on Qinshan_OUT_2.

(a) TEM micrograph. (b) Diffraction pattern of circle area.

Figure 4.12 shows the diffraction pattern of the outer layer. The polycrystalline group of Figure 4.12a was examined. The spottier ring pattern indicates the presence of the coarse grain in this layer. The grains have a typical size of about 0.06 to 0.09 μm . However, the large particles (0.7-0.9 μm) found by SEM observation were not observed in the outer layer by the TEM. It probably detached during the sample preparation step.

Table 4.8 The d-spacing values of outer layer on Qinshan Steel

Specimen No.	d-Spacing Value (nm)						
Qinshan_OUT_1	0.4870	0.2968	0.2559	-	0.1710	0.1622	0.1503
Qinshan_OUT_2	0.4852	0.2992	0.2551	0.2095	0.1716	0.1619	0.1505
Qinshan_OUT_3	0.4901	-	0.2564	0.2120	0.1723	0.1615	0.1491
Average	0.4874	0.2980	0.2558	0.2108	0.1716	0.1619	0.1500

The d-spacing in Table 4.8, fit the spinel structure of Fe_3O_4 very well. Chromium can also be found in this layer. The average ratio of Cr to Fe was of 0.018.

In summary, regardless of the particle size and contamination of nickel, both oxide layers were mainly Fe_3O_4 and contained trace amount of chromium in structure.

4.1.2.3 2.5% Cr / 1.0 Mo Steel

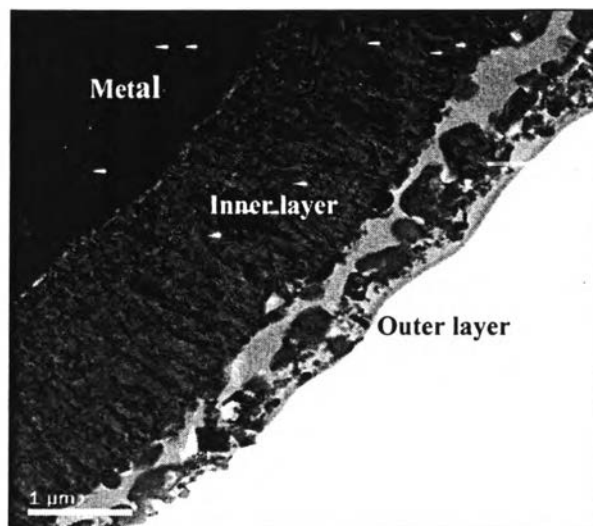
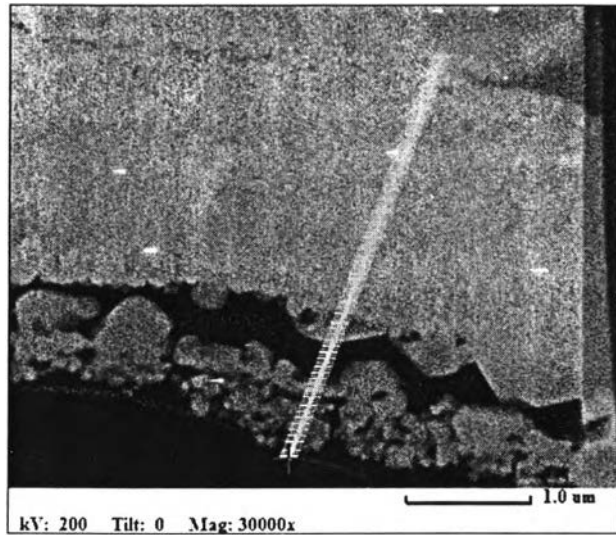


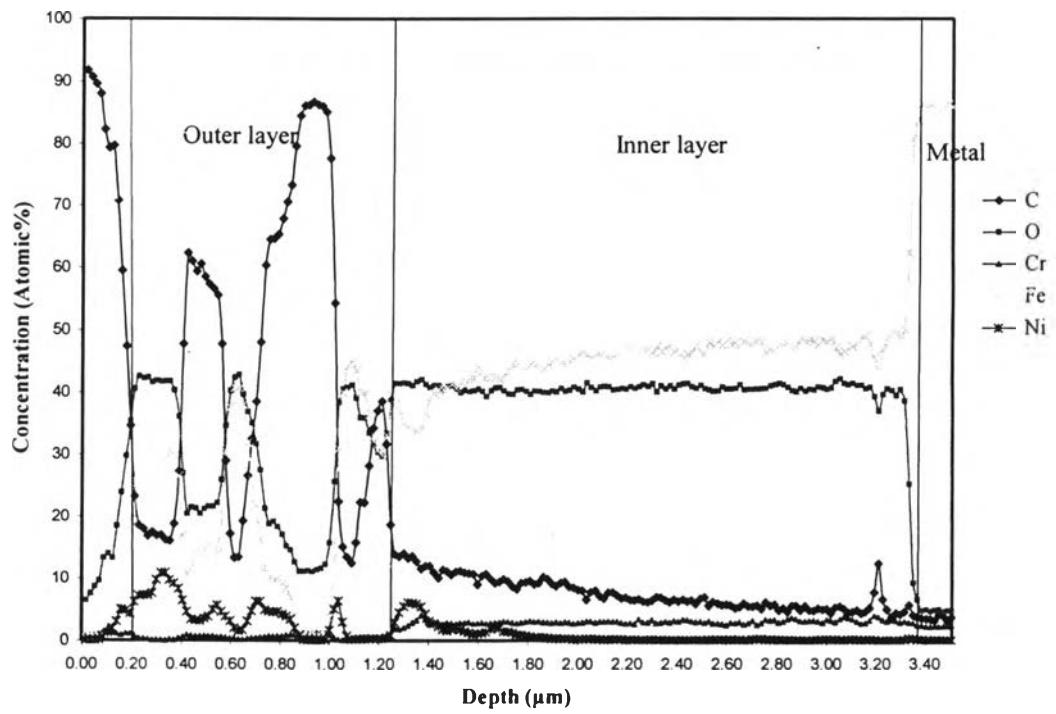
Figure 4.13 TEM micrograph showing the oxide film formed on 2.5%Cr / 1.0%Mo Steel.

Figure 4.13 shows the cross sectional observation of the oxide film developed on the 2.5%Cr / 1.0%Mo Steel. The oxide layer shows a double structure. A compact fine inner layer and loose outer layer can be observed.

The concentration depth profile in Figure 4.14 shows the presence of iron rich layer oxide in the inner layer. Fe and Cr concentrations in the outer layer itself were much lower than those in the inner layer. The nickel contamination is apparent in the outer layer. Other elements, P, S, Si, Ti, Mo and Mn, were also found but in ignored quantity. Again, the distribution of each element can be visualized by the EDX mapping as shown Figure 4.15. A chromium enrichment layer was observed in the inner layer while a nickel contamination was greater in the outer layer.



(a)

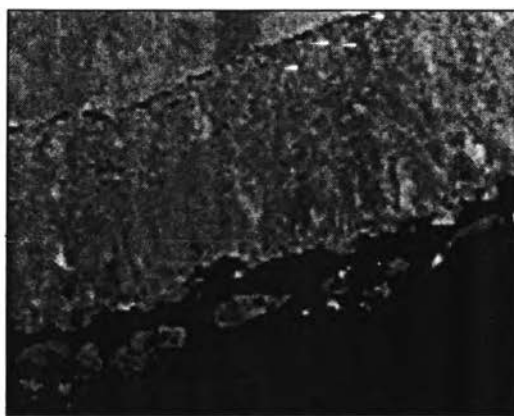


(b)

Figure 4.14 Line scanning result of 2.5%Cr / 1.0%Mo Steel.

(a) TEM micrograph with annotated line. (b) Depth profile from metal through the oxide layer.

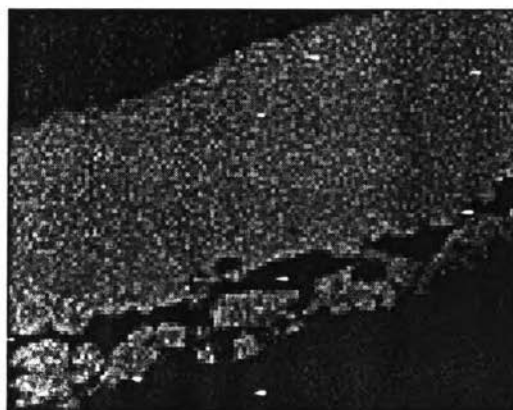
A sharp transition of Fe map in Figure 4.15 can be observed at the metal/oxide interface. The O map confirms the existence of inner and outer oxide film. The sharp transition of Cr indicates the enrichment of Cr in the inner layer and depletion of Cr in the outer layer. The Ni contamination can be seen at the outer layer.



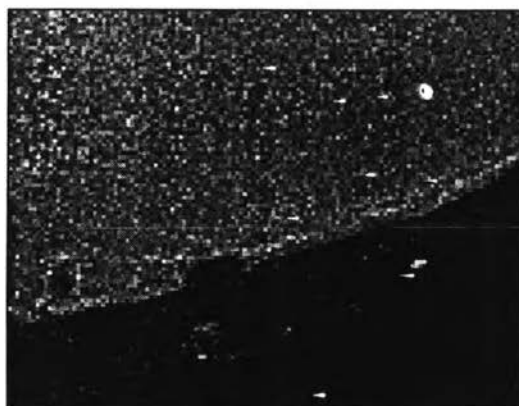
(a) Image



(b) Iron



(c) Oxygen



(d) Chromium



(e) Nickel

Figure 4.15 EDX mapping of 2.5%Cr / 1.0%Mo Steel.

a) Inner Layer

Chromium is formed in the inner layer. Based on the concentration depth profile in Figure 4.14b, the atomic ratio of Cr to Fe was about 0.065 on average. The oxide thickness was about 2.1 μm . The identification of its crystal structure was achieved by the electron diffraction pattern.

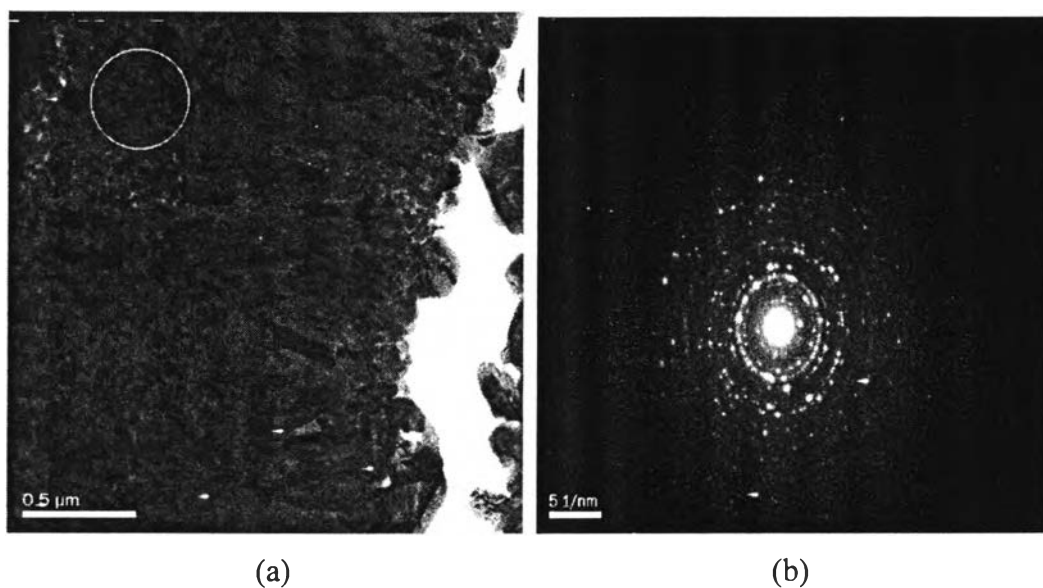


Figure 4.16 TEM micrograph of inner oxide layer with electron diffraction pattern of oxide layers developed on 2.5% Cr_IN_3.

(a) TEM micrograph. (b) Diffraction pattern of circle area shown in (a).

TEM micrograph and electron diffraction pattern of the inner layer is shown in Figure 4.16. The d-spacing values are summarized in Table 4.9.

Table 4.9 The d-spacing values of inner layer on 2.5%Cr / 1.0%Mo Steel

Specimen No.	d-Spacing Value (nm)						
2.5%Cr_IN_1	0.4908	0.3026	0.2565	0.2162	0.1748	0.1647	0.1514
2.5%Cr_IN_2	0.4971	0.3019	0.2573	0.2130	-	0.1647	-
2.5%Cr_IN_3	0.4905	0.2996	0.2566	0.2132	0.1724	0.1629	0.1500
Average	0.4928	0.3013	0.2568	0.2141	0.1736	0.1641	0.1507

In comparison with the d-spacing values of Fe_3O_4 in Table 4.5, the d-spacing values of the inner layer were of the Fe_3O_4 structure. However, the concentration depth profile and EDX map had shown the existence of chromium ($\text{Cr}/\text{Fe} = 0.065$). The Cr^{3+} can substitute the position of Fe^{3+} inside the spinel structure. Therefore, the inner oxide structure is assumed to be $(\text{Fe}^{2+})(\text{Fe}^{3+}, \text{Cr}^{3+})_2\text{O}_4$.

b) Outer Layer

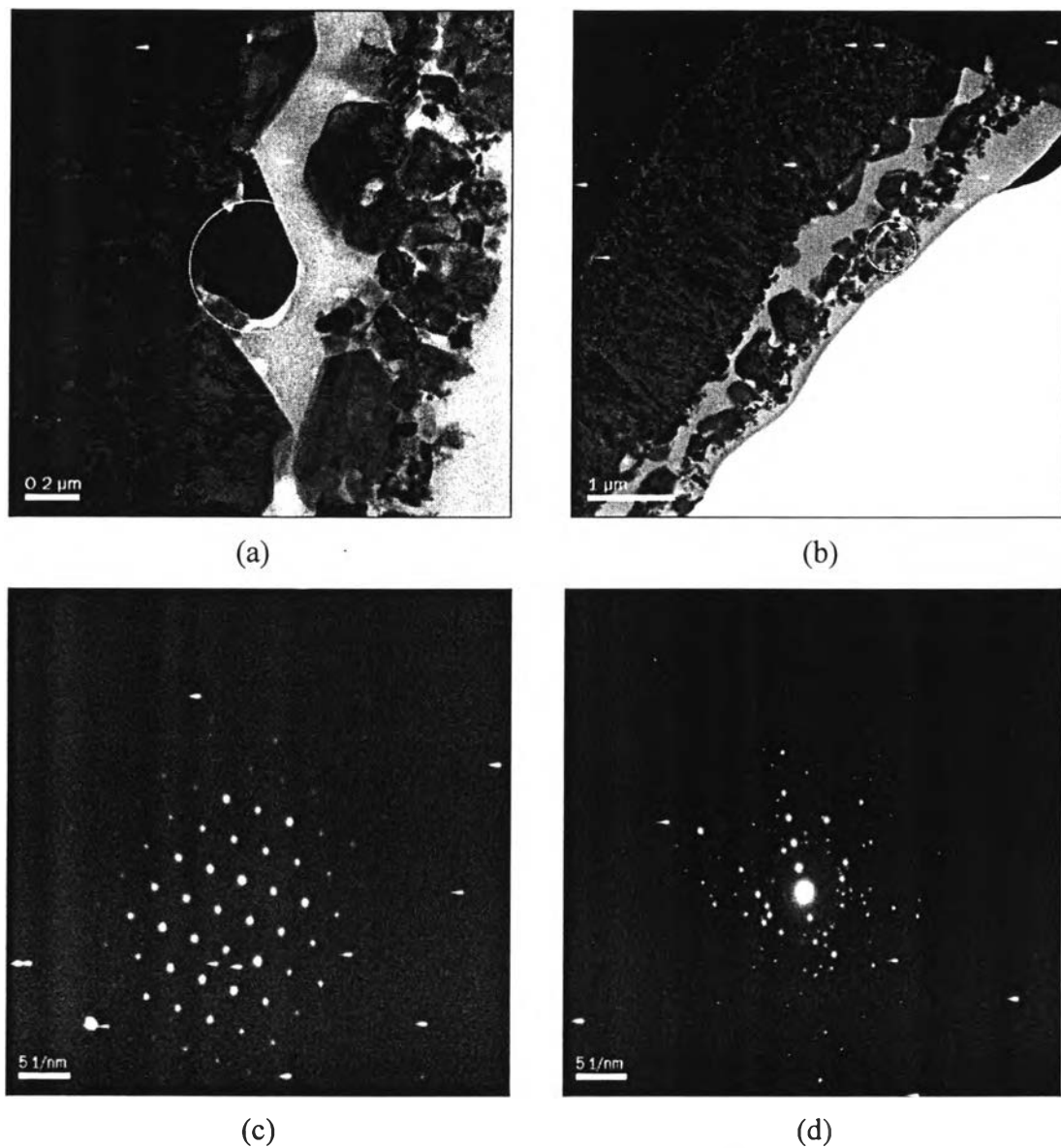


Figure 4.17 TEM micrograph of outer layer on 2.5 %Cr / 1.0%Mo Steel with electron diffraction pattern.

(a) TEM micrograph of large oxide particles developed on 2.5% Cr_OUT_3

(b) TEM micrograph of small oxide particles developed on 2.5% Cr_OUT_1

(c) Diffraction pattern of circle area shown in (a)

(d) Diffraction pattern of circle area shown in (b)

Figure 4.17 shows the TEM micrographs with electron diffraction pattern of the outer layer. This layer contained relatively large oxide particles and small oxide particles. The oxide particle ranged between 0.05 and 0.45 μm , which is consistent with the grain size of the SEM observation on the surface. The large single particle in Figure 4.17a gave the single crystal pattern in Figure 4.17b that can be confirmed. It was a single crystal and not a fracture of the fine grain inner layer. The diffraction pattern of Figure 4.17a corresponds to the Fe_3O_4 structure. Similarly, the polycrystalline group of small oxide particles also gave a good fit to Fe_3O_4 structure. The d-spacing of others samples are summarized in Table 4.10.

Table 4.10 The d-spacing values of outer layer of 2.5%Cr / 1.0%Mo Steel

Specimen No.	d-Spacing Value (nm)						
2.5 %Cr_OUT_1	0.4912	0.3032	0.2533	0.2445	0.2102	-	0.1696
2.5 %Cr_OUT_2	0.4913	0.2938	0.2531	0.2454	-	0.1943	-
2.5 %Cr_OUT_3	0.4886	0.3037	0.2578	0.2453	0.2146	0.1948	-
Average	0.4904	0.3002	0.2547	0.2451	0.2124	0.1945	0.1696

The EDX map in Figure 4.15e revealed the occurrence of nickel contamination at the outer oxide layer. The average ratio of Ni to Fe was 0.17 on average. Small amount of Cr (Cr/Fe = 0.025) can also be detected. Thus, Cr and Ni can possibly substitute the iron in the spinel structure, resulting in the $(\text{Fe}^{2+}, \text{Ni}^{2+})(\text{Fe}^{3+}, \text{Cr}^{3+})_2\text{O}_4$ structure.'

In summary, It is concluded that the inner oxide layer is the Fe_3O_4 structure and contained chromium ($\text{Cr}/\text{Fe} = 0.065$) or chromium iron oxide. The outer oxide layer, regardless of the size and contamination of nickel, is also Fe_3O_4 structure, but with lower Cr content ($\text{Cr}/\text{Fe} = 0.025$).

4.1.2.4 304SS

The cross-sectional micrograph observed by TEM for 304SS is shown in Figure 4.18. The film had a double layer structure similar to previous specimens. The fine grain inner layer and large single oxide particles can be observed.

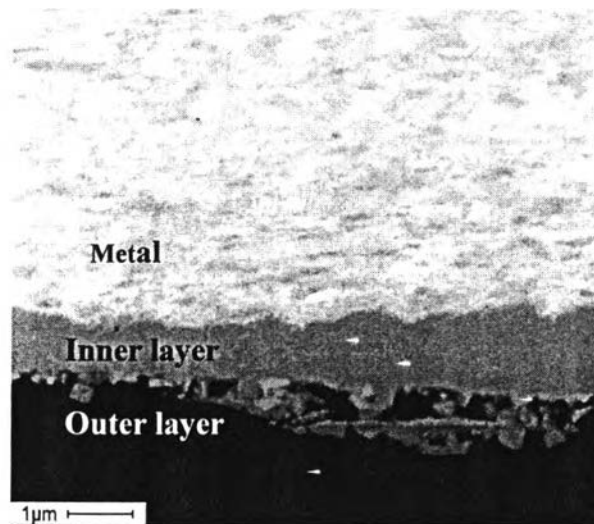
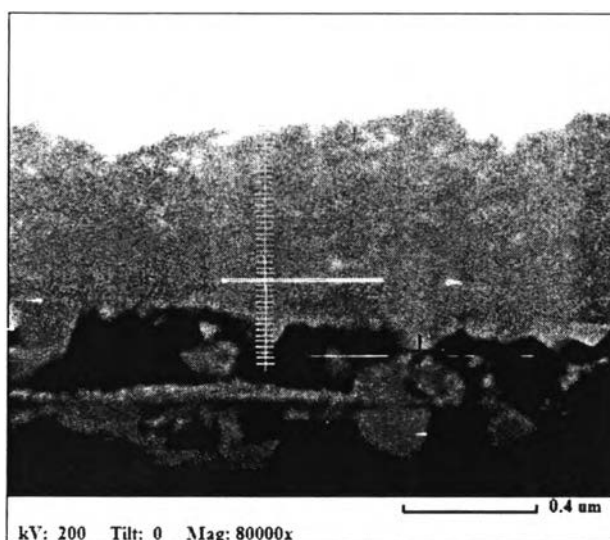
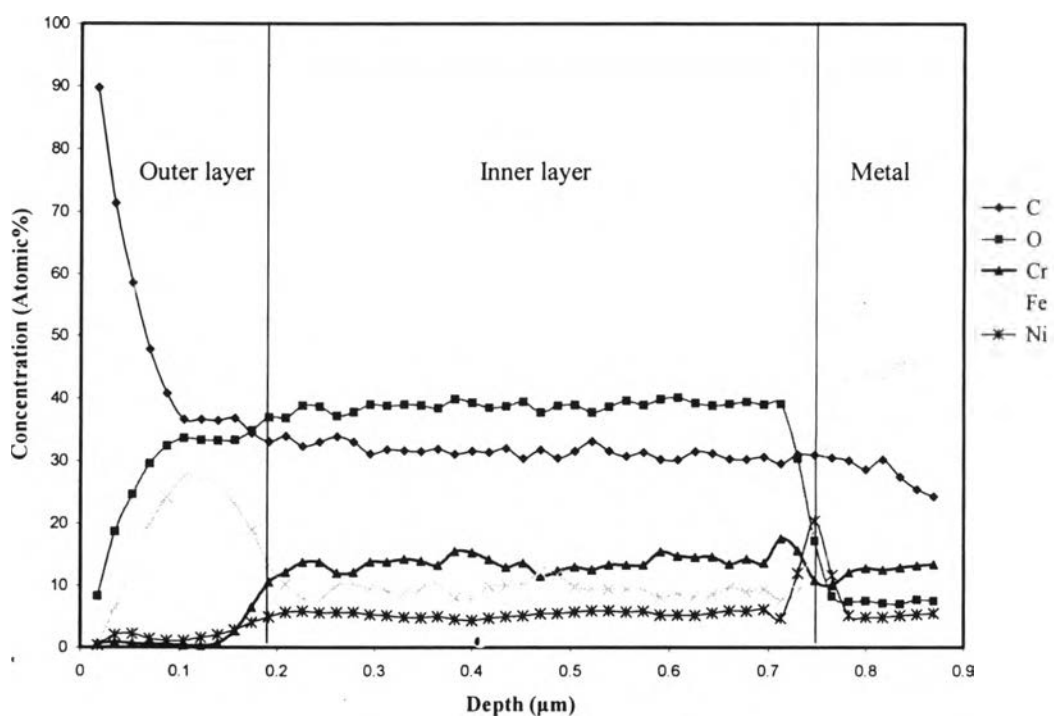


Figure 4.18 TEM micrograph showing the oxide morphology formed on 304SS.



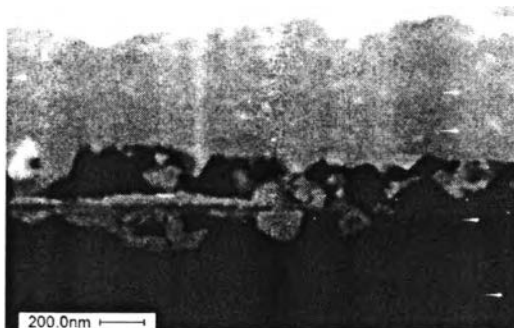
(a)



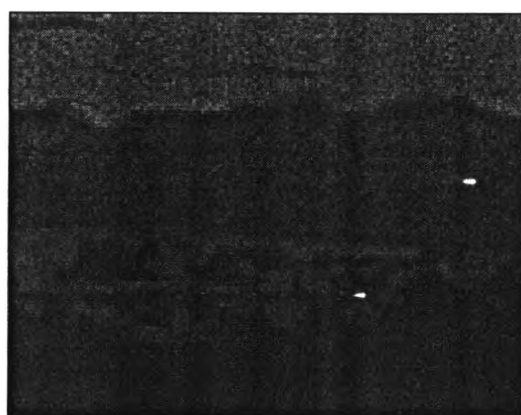
(b)

Figure 4.19 Line Scanning result of 304SS.

(a) TEM micrograph with annotated line. (b) Depth profile from metal through the oxide layer.



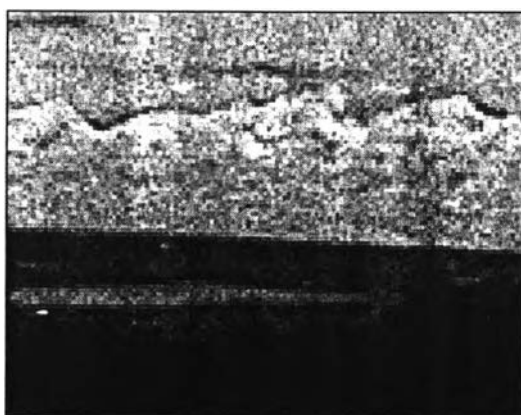
(a) Image



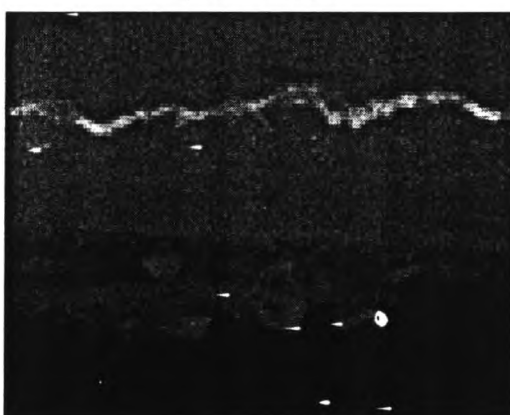
(b) Iron



(c) Oxygen



(d) Chromium



(e) Nickel

Figure 4.20 EDX mapping of 304SS.

The concentration depth profile in Figure 4.19b and the Cr map in Figure 4.20d indicate the chromium enrichment in the inner layer. The atomic ratio of Cr to Fe ratio was 1.48, whereas the ratio of Ni to Fe was of 0.58 on average. The Ni enrichment at the metal/oxide interface can be observed on the Ni map. The outer layer was enriched in Fe and depleted in Cr. The Cr to Fe and Ni to Fe ratios were of 0.076 and 0.10 on average, respectively. The crystal structure of both layers can be determined by the electron diffraction pattern.

a) Inner Layer

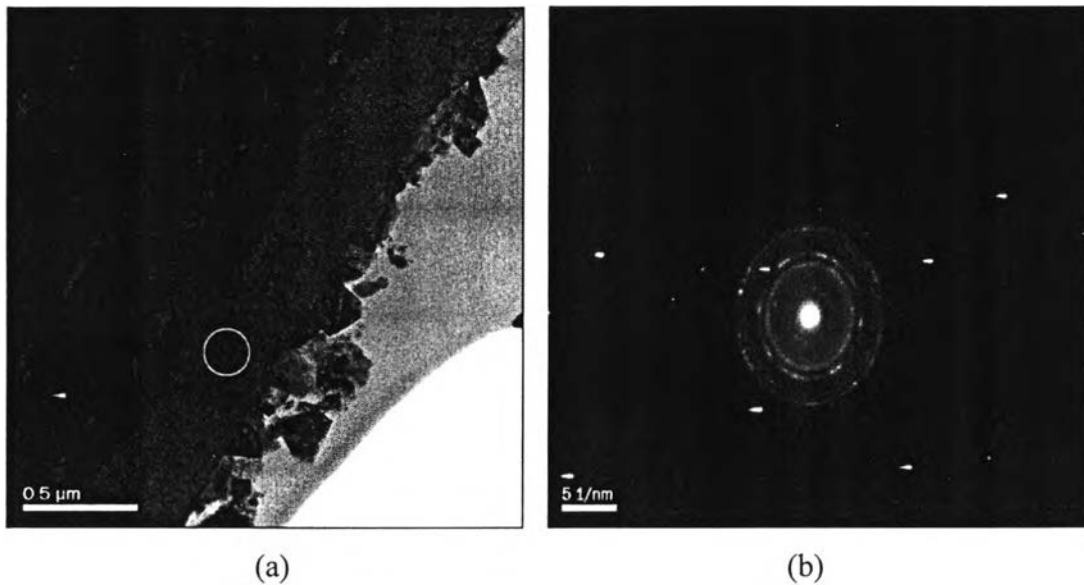


Figure 4.21 TEM micrograph of inner oxide layer with electron diffraction pattern of oxide layers developed on 304SS_IN_2.

(a) TEM micrograph (b) Diffraction pattern of circle area shown in (a)

Figure 4.21 shows the diffraction pattern of the inner oxide layer. The continuous ring pattern revealed the very small size of oxide particles. The diffraction pattern of the fine-grain, continuous layer corresponded to the spinel structure. All d-spacing results of the inner layer are summarized in Table 4.11.

Table 4.11 The d-spacing values of inner layer on 304SS

Specimen N o.	d-Spacing Value (nm)						
304SS_IN_1	0.4859	0.2526	0.2167	0.1714	0.1654	0.1533	0.1318
304SS_IN_2	0.4924	0.2566	0.2128	-	-	0.1507	-
Average	0.4892	0.2546	0.2147	0.1714	0.1654	0.1520	0.1318

Due to the presence of chromium and nickel ($\text{Cr/Fe} = 1.48$, $\text{Ni/Fe} = 0.58$), the structure is assumed to be $(\text{Ni}^{2+}, \text{Fe}^{2+})(\text{Cr}^{3+}, \text{Fe}^{3+})_2\text{O}_4$. Significantly, Cr was the most enriched specie of the inner oxide layer.

b) Outer Layer

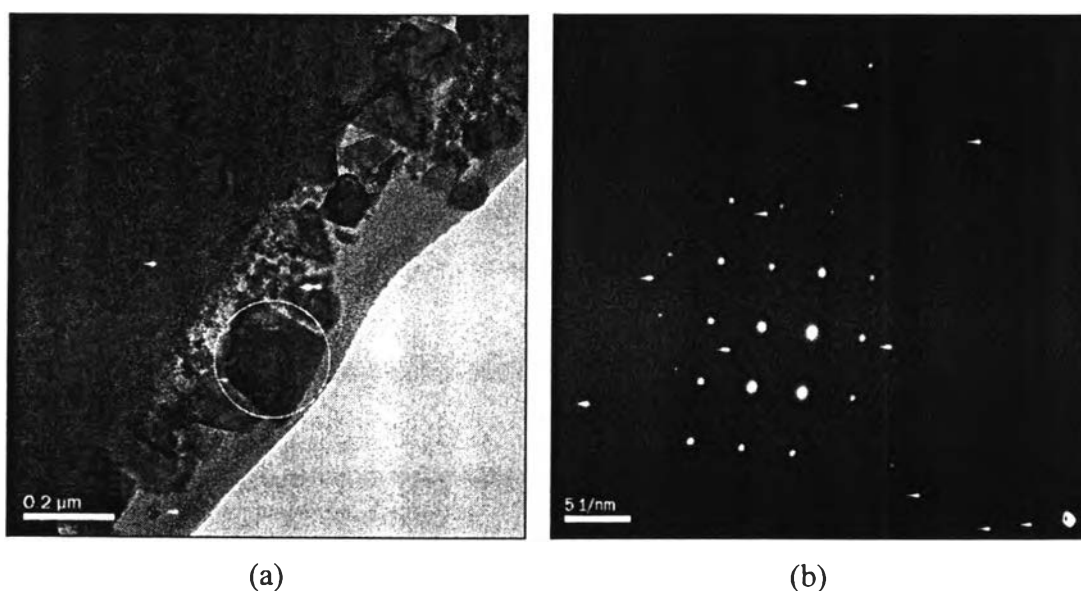


Figure 4.22 TEM micrograph of outer oxide layer with electron diffraction pattern of oxide layers developed on 304SS_2_OUT.

(a) TEM micrograph. (b) Diffraction pattern of circle area shown in (a).

Figure 4.22 shows the TEM micrograph and single crystal pattern of large oxide particles at the outer layer. The grain size of the outer layer was between 0.002-0.48 μm in range. The d-spacing values in Table 4.12 showed a good agreement with the spinel structure.

Table 4.12 The d-spacing values of outer layer on 304SS

Specimen No.	d-Spacing Value (nm)						
304SS_OUT_1	-	-	0.2585	-	0.1940	0.1751	-
304SS_OUT_2	-	0.3000	-	-	-	-	0.1678
304SS_OUT_3	0.4883	0.2911	-	0.2490	0.1920	0.1744	0.1627
Average	0.4883	0.2955	0.2585	0.2490	0.1930	0.1747	0.1653

The concentration depth profile indicates the iron-rich oxide contained nickel and was depleted in chromium ($\text{Cr/Fe} = 0.05$, $\text{Ni/Fe} = 0.08$). However, the nickel can probably be attributed to contamination, which was found for other steels.

From TEM analysis, it is seen that the oxide film on the steels with lower chromium content contained less chromium as shown in Figure 4.23. It is reasonably assumed that Cr concentration in the inner oxide film is from the base metal composition.

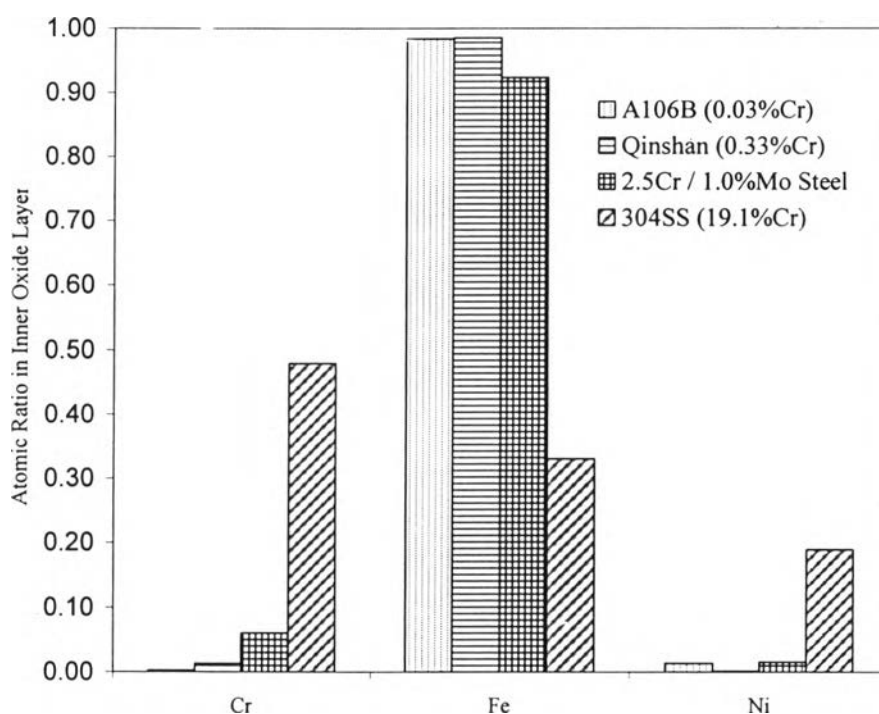


Figure 4.23 Atomic ratio in the inner oxide layer.

Figure 4.24 shows the cation ratio in the outer oxide layer. Apparently, Cr was depleted in the outer oxide layer. A large content of Ni is also the contamination in the system.

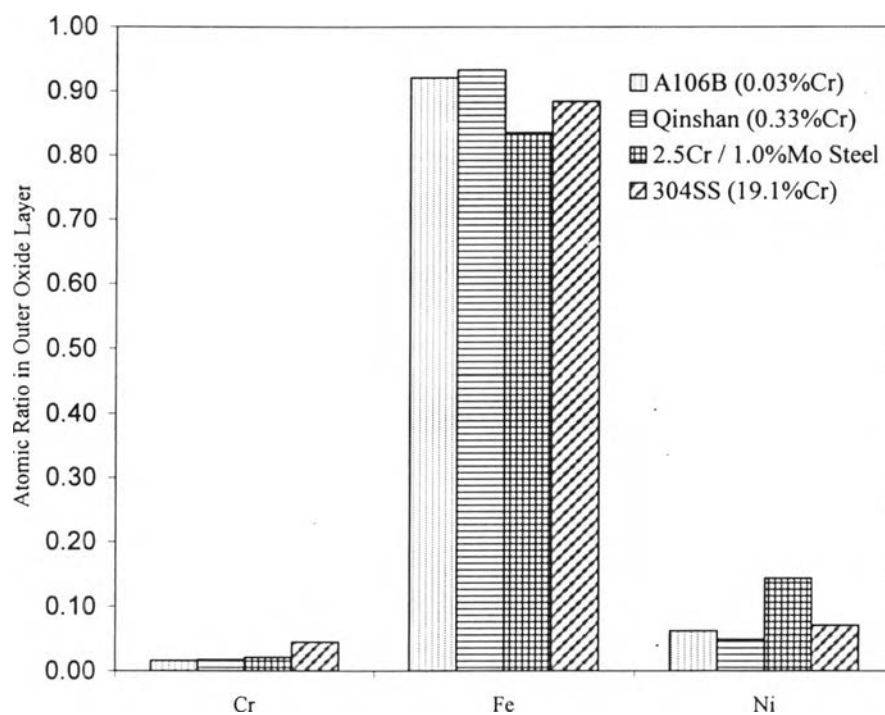
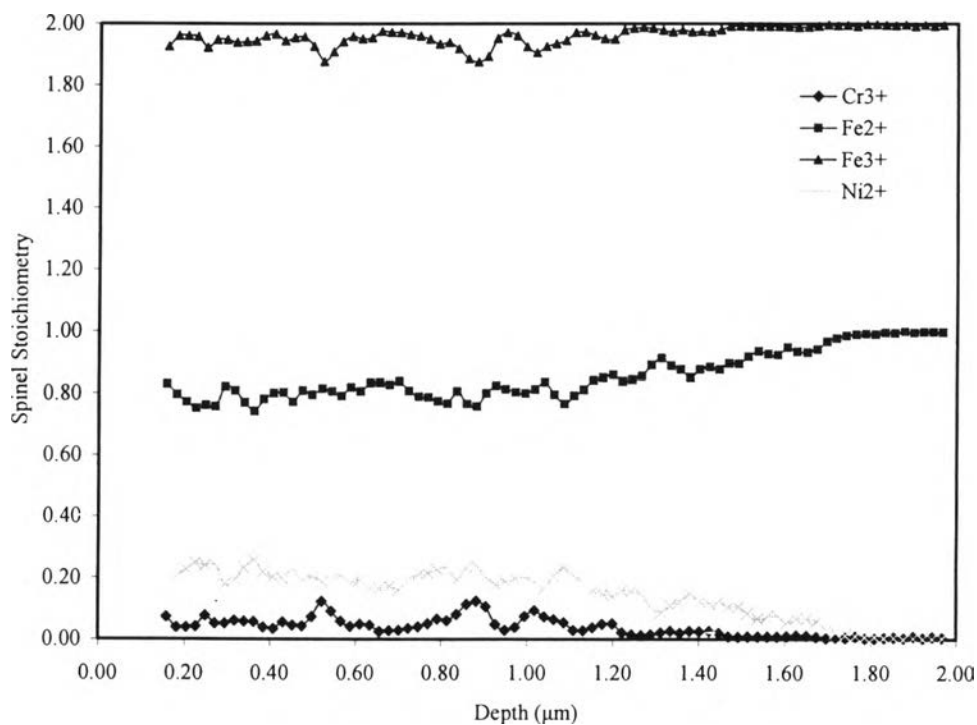


Figure 4.24 Atomic ratio in the outer oxide layer.

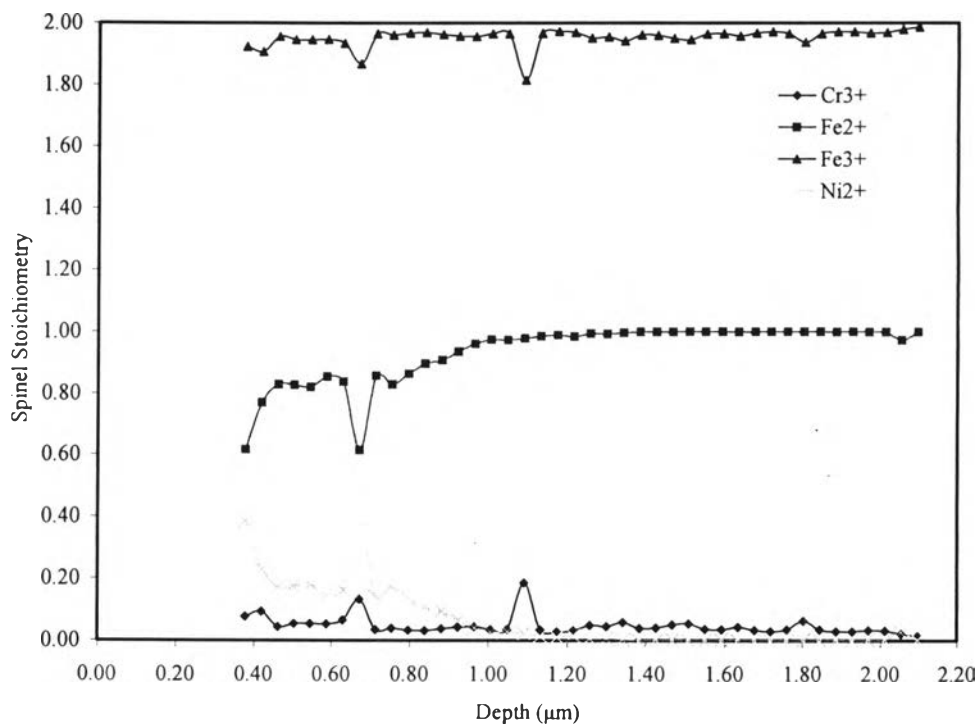
The enrichment of Cr and Ni in the inner oxide layer can be explained by the diffusion rate of metal ions in the spinel lattice. Robertson (1989) reported the diffusion of metal ions to follow the order $Fe^{3+} > Fe^{2+} > Ni^{2+} > Cr^{3+}$. The chromium and nickel move more slowly and thus enrich in the inner layer.

As discussed, the electron diffraction pattern revealed that the microstructure of the oxide film developed on all studied steels during exposure to high temperature water as the spinel structure. Spinel is an oxide of the type AB_2O_4 where $A = Fe^{2+}$ and Ni^{2+} and $B = Fe^{3+}$ and Cr^{3+} . Ni^{2+} can substitute the position of Fe^{2+} because their charge and ionic radii are close each other. Similarly, Cr^{3+} can substitute the Fe^{3+} in the spinel lattice. The ionic radii of Fe^{2+} , Ni^{2+} , Fe^{3+} and Cr^{3+} are 0.74, 0.69, 0.64 and 0.63, respectively. Thus, the possible crystal structures include Magnetite (Fe_3O_4), Chromite ($FeCr_2O_4$) and Nickel Ferrite ($NiFe_2O_4$). Because the crystal lattice of all structures being face centered cubic and the lattice size being similar (0.8396 nm for Fe_3O_4 , 0.8379 nm for $FeCr_2O_4$ and 0.833 for $NiFe_2O_4$), the values of d-spacing are similar as well. Therefore, it is difficult to distinguish the three crystal structures based on TEM results. However, it is possible to do the

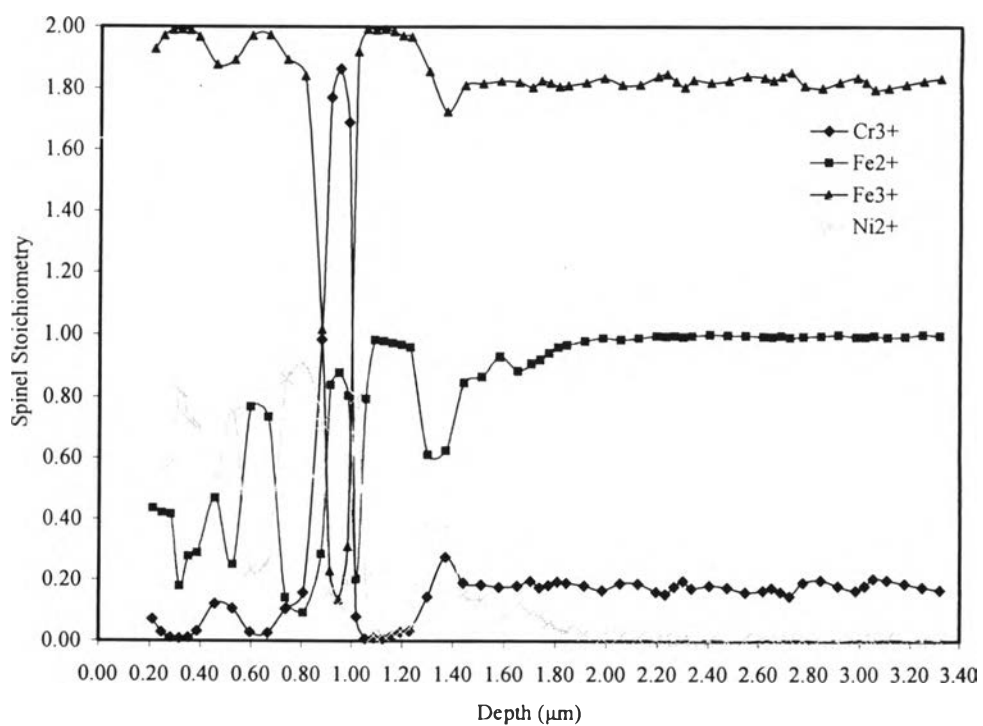
qualitative analysis based on the results of the diffraction pattern that indicates a spinel structure that assumed chromium was present as Cr^{3+} and nickel as Ni^{2+} . Figure 4.25 shows the spinel stoichiometry of Cr^{3+} , Fe^{2+} , Fe^{3+} and Ni^{2+} for all tested steels. The stoichiometry of Fe^{2+} and Fe^{3+} can be calculated by the charge and material balance of Fe (EDXA can not distinguish Fe^{2+} from Fe^{3+}). By Integrating area yields a quantitative analysis of each element.



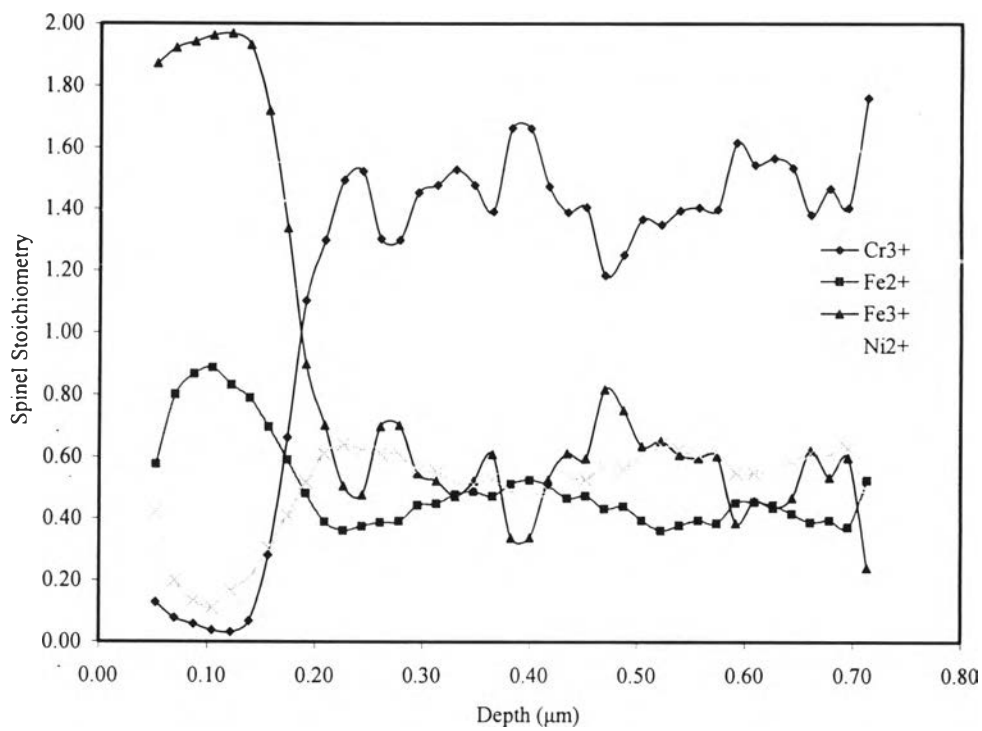
(a) A106B (0.03%Cr)



(b) Qinshan (0.33%Cr)



(C) 2.5%Cr / 1.0 %Mo Steel



(d) 304SS (19.1%Cr)

Figure 4.25 Spinel Stoichiometry of Cr³⁺, Fe²⁺, Fe³⁺ and Ni²⁺

Table 4.13 Spinel composition $(\text{Ni}_x\text{Fe}_{1-x})(\text{Fe}_{2-y}\text{Cr}_y)\text{O}_4$ of inner oxide and outer oxide layer

Specimen	Inner Layer		Outer Layer	
	X	Y	X	Y
A106B (0.03%Cr)	0.0	0.0	0.2	0.0
Qinshan (0.33%Cr)	0.0	0.0	0.1	0.1
2.5%Cr / 1.0%Mo Steel	0.0	0.2	0.4	0.1
304SS (19.1%Cr)	0.6	1.4	0.2	0.1

Table 4.13 shows the stoichiometry of the spinel structure $(\text{Ni}_x\text{Fe}_{1-x})(\text{Fe}_{2-y}\text{Cr}_y)\text{O}_4$, which was quantified by the numerical integration. The results show that the inner layer on A106B and Qinshan steels was Fe_3O_4 type. A significant amount of Cr was detected in the inner oxide larger on 2.5%Cr / 1.0%Mo steel. The inner oxides on 2.5%Cr / 1.0%Mo steel and 304SS were $\text{Fe}(\text{Fe}_{0.9}\text{Cr}_{0.1})_2\text{O}_4$ and $(\text{Ni}_{0.6}\text{Fe}_{0.4})(\text{Fe}_{0.3}\text{Cr}_{0.7})_2\text{O}_4$, respectively.

The grain size of the inner oxide layer was too small to measure, however the electron diffraction pattern can be used for qualitative comparison. A higher degree of continuous ring pattern refers to the smaller grain size. Figure 4.26 shows the electron diffraction pattern of the inner oxide layer for all steels. It is shown that the diffraction pattern of 304SS had the most continuous ring pattern. The oxide film on the steel containing higher chromium content tend to have higher degree continuous ring pattern, 2.5%Cr / 1.0%Mo steel > Qinshan > A106B.

Regarding with the concentration depth profile and the appearance of electron diffraction pattern, it can be concluded that the enrichment of the Cr in the innermost layer resulting in a change of morphology of the inner oxide film. The higher Cr content steel can give the finer grain size and more compact layer relative to the lower Cr content steel. These results were consistent with the SEM results.

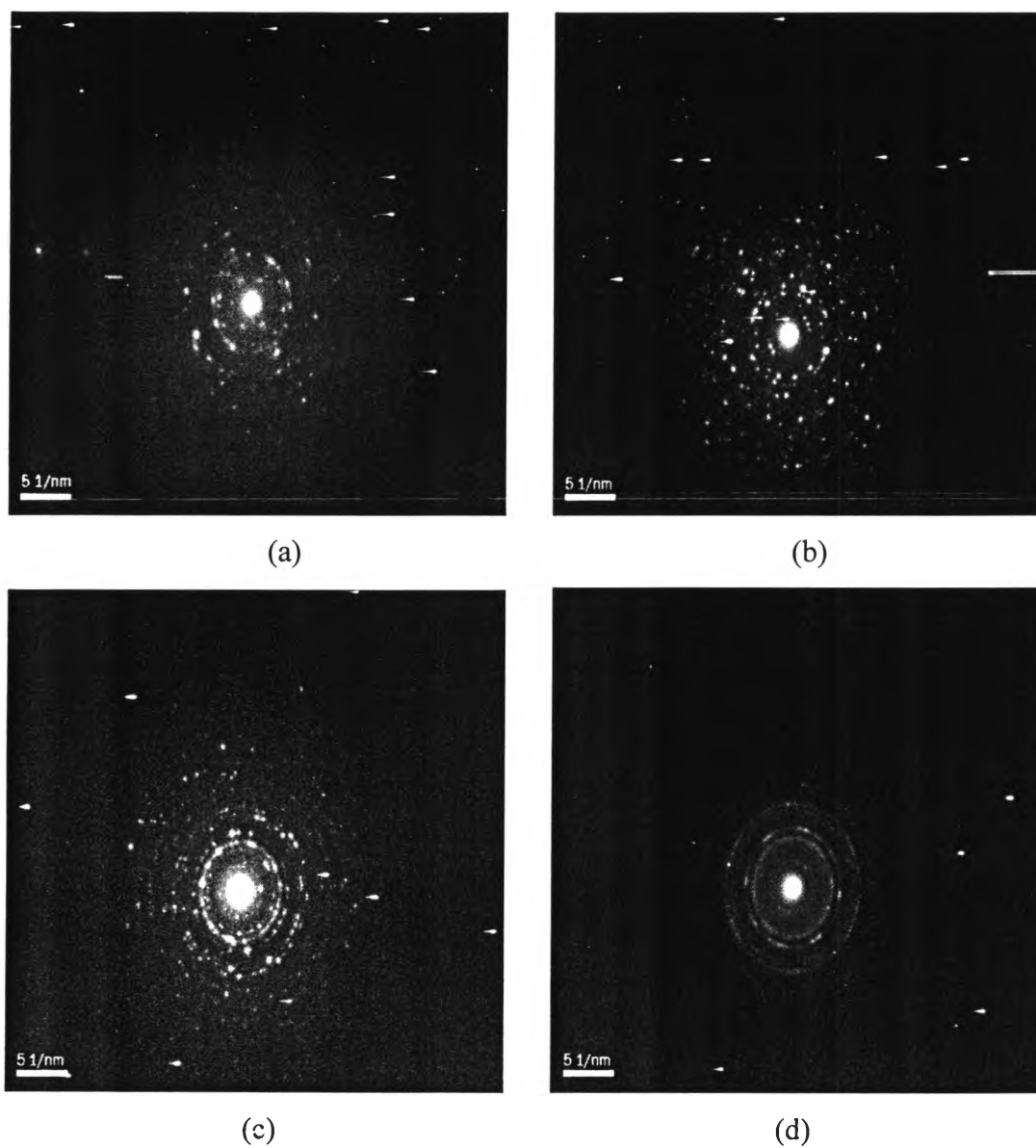


Figure 4.26 Electron Diffraction Pattern of inner oxide layer in each material.

(a) A106B (0.03%Cr) (b) Qinshar (0.33%Cr)

(c) 2.5%Cr / 1.0%Mo steel (d) 304SS (19.1%Cr)

4.2 Electrochemical Characterization

The electrochemical technique i.e., polarization curve and Electrochemical Impedance technique, were used to characterize the oxide films on steels.

4.2.1 Polarization Curve Analysis

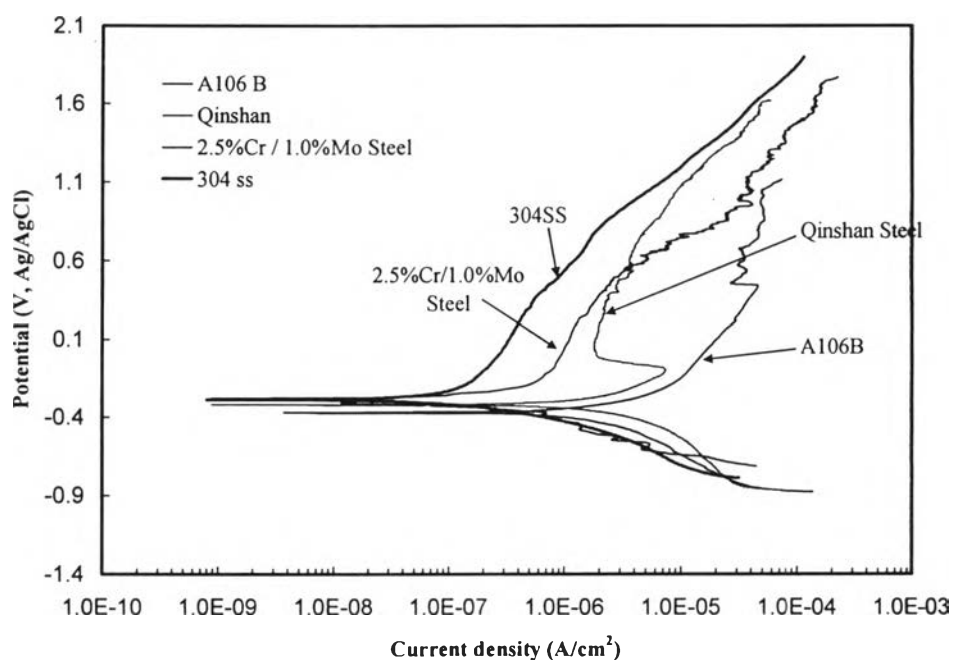


Figure 4.27 Polarization Curves obtained for A106B (0.03%Cr), Qinshan (0.33%Cr), 2.5%Cr / 1.0%Mo Steel and 304SS (19%Cr), in alkaline environment (LiOH, pH 10.5) at room temperature and scan rate of 0.5 mv/s.

Figure 4.27 shows the polarization curves obtained after immersion of the pre-filmed steels in water solution (pH 10.5). The sweep potential was carried out in the positive direction at -0.5 V to 2.0 V versus corrosion potential (E_{corr}) at a scanning rate of 0.5 m/s.

After immersion the pre-filmed samples in the solution, the steel will be corroded under the restriction of the existence oxide film. The corrosion rate of iron at each applied potential value can be measured in terms of the current

density. It is seen from Figure 4.27 that the anodic current density decreases with increasing Cr content in steel.

It is seen that 304SS has the highest corrosion resistance, while the A106B carbon steel is the least resistant to corrosion. It, therefore, revealed that the Cr content has a significant effect on the corrosion resistance of steels. The higher Cr content provides a greater corrosion resistance.

4.2.2 Electrochemical Impedance Analysis

Electrochemical Impedance Spectroscopy is a technique; use to describe the corrosion behavior of such a system by fitting the impedance results with the equivalent circuit.

Figure 4.28 and Figure 4.29 show the typical Nyquist and Bode diagrams obtained at the corrosion potential (E_{corr}). The two semicircles exist in the Nyquist diagram, indicating two electrochemical reactions at steel/oxide interface and oxide/solution interface.

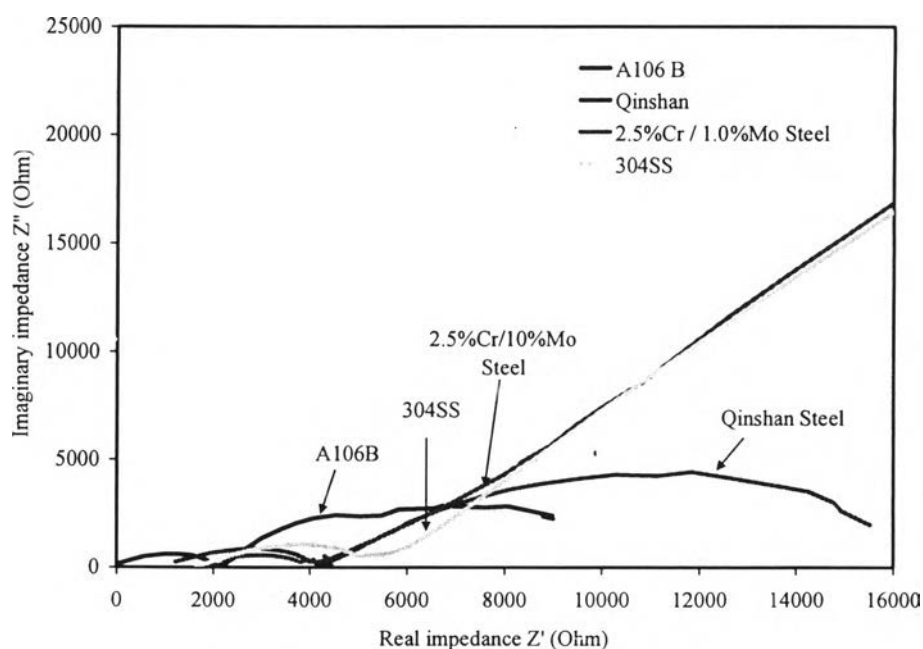
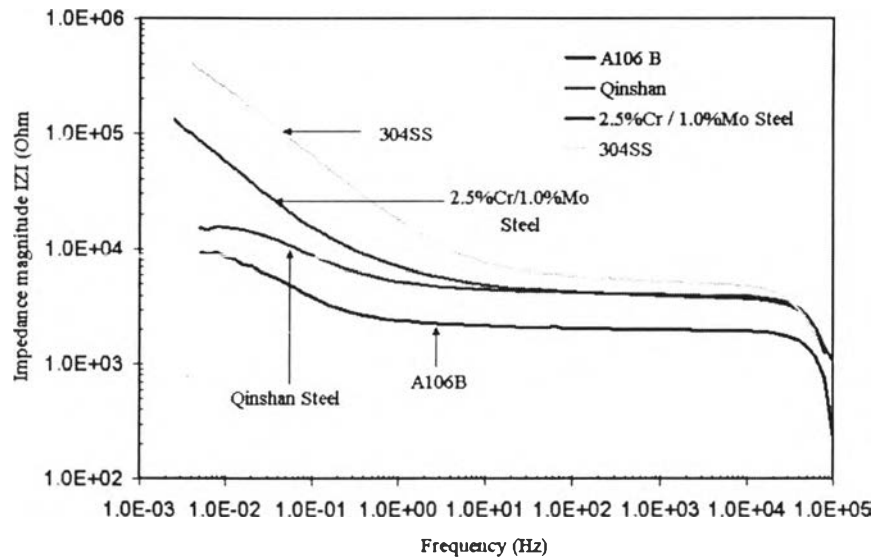
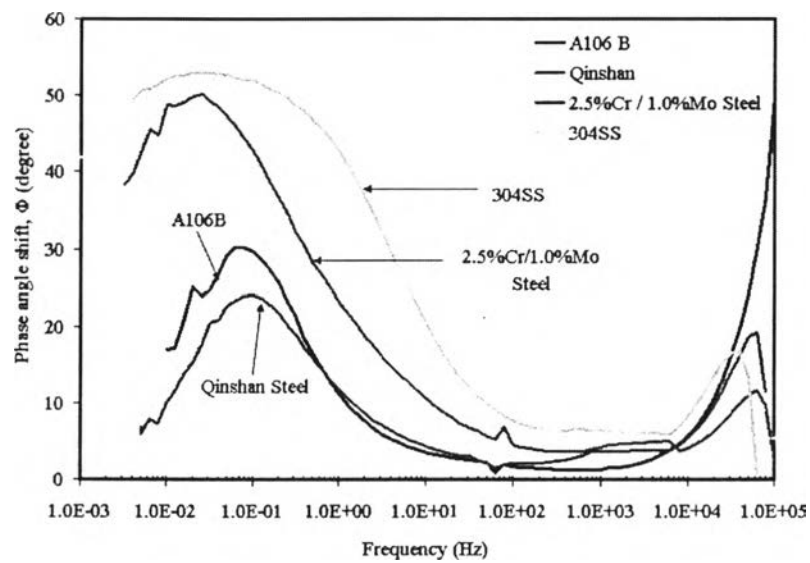


Figure 4.28 Nyquist diagram obtained for A106B, Qinshan, 2.5%Cr / 1.0%Mo Steel and 304SS in LiOH solution (pH 10.5), at room temperature



(a)



(b)

Figure 4.29 Bode diagrams obtained for A106B, Qinshan, 2.5%Cr / 1.0%Mo Steel and 304SS in LiOH solution (pH 10.5), at room temperature.

(a) $\log |Z|$ versus frequency

(b) phase angle versus frequency

A typical equivalent circuit corresponding to the corrosion process occurring on filmed cover steel is shown in Figure 4.30.

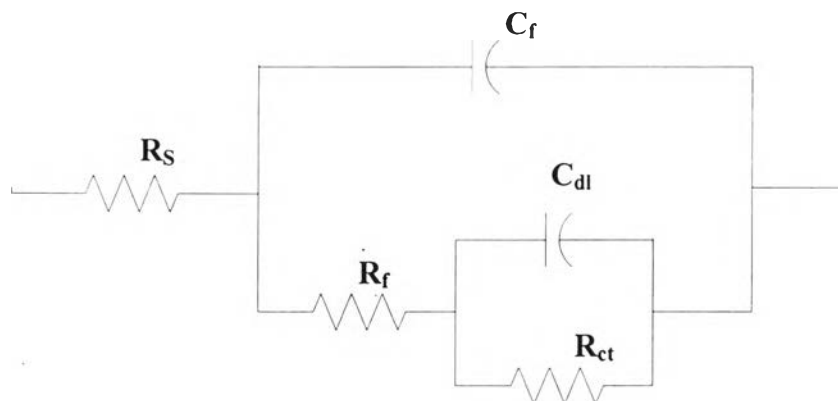


Figure 4.30 Equivalent circuit used to fit the experimental data of EIS diagram for A106B, Qinshan, 2.5%Cr / 1.0%Mo Steel and 304SS in LiOH solution (pH 10.5), at room temperature.

The circuit element in Figure 4.31 contains, solution resistance (R_s), charge transfer resistance (R_{ct}), double layer capacitance (C_{dl}), oxide film resistance (R_f) and oxide film capacitance (C_f). The terms R_f and C_f come from the dissolution reaction of oxide film, while R_{ct} and C_{dl} reflects the Fe corrosion at oxide/steel interface. Table 4.14 summarizes the parameters value for the circuit, which best fit the experimental impedance diagrams.

Table 4.14 Values of equivalent circuit elements used for best fit to impedance diagrams of A106B, Qinshan, 2.5%Cr / 1.0%Mo Steel and 304SS in LiOH solution (pH 10.5), at room temperature

Steels	$R_{ct} (\Omega \text{ cm}^2)$	$C_{dl} (\mu\text{F}/\text{cm}^2)$	$R_f (\Omega \text{ cm}^2)$	$C_f (\text{nF}/\text{cm}^2)$
A106 B	6131.2	693.0	781.2	7.9
Qinshan Steel	10,882.0	339.0	1204.8	5.9
2.5% Cr / 1.0%Mo Steel	123,200.0	177.0	1213.5	329
304SS	455,384.4	36.0	2029.2	76.7

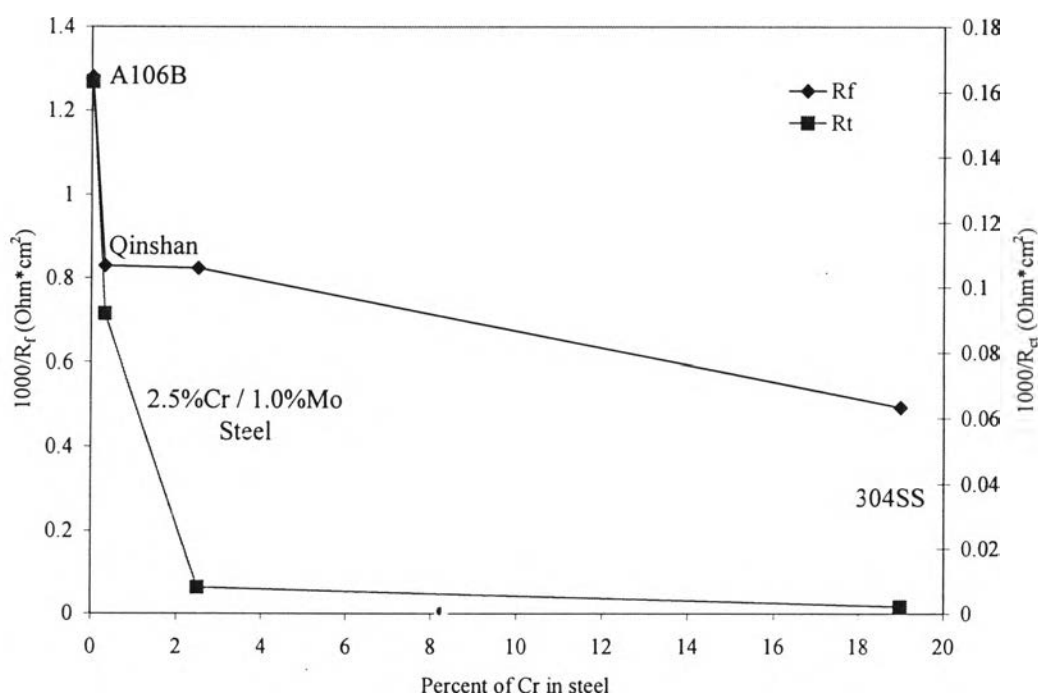


Figure 4.31 Charge transfer resistance and Oxide film resistance (obtained in LiOH, pH 10.5, room temperature) as a function of different content of Cr modified in steels.

The value of R_{ct} indicates the resistance of Fe to corrosion at the steel/oxide interface. The value of R_f is related to the film porosity. The low value of R_f means that there is a low diffusion resistance of oxide film.

Figure 4.31 shows the relationship between the inverse value of charge transfer resistance (R_{ct}^{-1}) and oxide film resistance (R_f^{-1}) with different Cr content steels. The value of R_{ct}^{-1} was proportional to the corrosion rate. Based on the results, 304SS had the lowest value of R_{ct}^{-1} , therefore 304SS had a lowest corrosion rate relative to the lower Cr content steels. The result was consistent with the passive current density obtained from the polarization curve in Figure 4.27. For the relationship between R_f^{-1} with different materials, the result was in the same manner with R_{ct}^{-1} . The steel containing higher Cr content gave a smaller value of R_f^{-1} which means the dissolved ions can more easily diffuse through the oxide film of the steels containing lower Cr content or had a larger value of porosity relative to steel containing a higher Cr content. The result was consistent with the surface characterization results that indicated the higher Cr content steel provides a finer grain size and more compact layer.

It can be noticed that the charge transfer resistance was substantially increased from A106B to 2.5%Cr / 1.0%Mo steel, while an increase of R_{ct} from 2.5%Cr / 1.0%Mo steel was less. The low value of R_f , relative to R_{ct} , indicated that the oxide film developed under the flow-assisted corrosion conditions, does not give a good protective film.